# Renewable Monomer Feedstocks via Olefin Metathesis: Fundamental Mechanistic Studies of Methyl Oleate Ethenolysis with the First-Generation Grubbs Catalyst

Kenneth A. Burdett, Lori D. Harris, Peter Margl, Bob R. Maughon,* Tezi Mokhtar-Zadeh, Peter C. Saucier, and Eric P. Wasserman

*Corporate Research and Development, The Dow Chemical Company, 1776 Building, Midland, Michigan 48674*

*Received September 18, 2003*

The conversion of seed oil based feedstocks such as methyl oleate into useful commercial raw materials via olefin metathesis has been a research focus for decades, due to their low cost and renewable supply, but technical success has been limited due to poor catalyst activities and turnovers. We report here recent studies on the cross-metathesis of methyl oleate with ethylene (ethenolysis) catalyzed by bis(tricyclohexylphosphine)benzylideneruthenium dichloride (**1**). At 25 °C/60 psig of ethylene, catalysis by **1** results in the highly selective formation of 1-decene and methyl 9-decenoate. However, reactivity losses limit the catalyst turnovers well below commercial viability in batch reactor operation. In an attempt to address the limitations of this chemistry, a combination of an experimental evaluation of the impact of process parameters, a detailed analysis of the fundamental reaction steps, kinetic modeling, and molecular modeling has been applied to develop a more detailed understanding of this complex catalytic pathway. These fundamental studies have led to a more complete understanding of the factors impacting catalyst performance and the identification of approaches necessary to achieve an economically viable process.



## Introduction

The production of useful commercial raw materials from renewable natural resources is a focus currently throughout both the chemical industry and academia, as issues of both price and availability of fossil fuel derived feedstocks become more pressing.[1,2] However, this strategic shift toward evaluating previously underutilized renewable resources will require several key breakthroughs to achieve commercial realization. First, renewable feedstocks must be identified which can meet economic targets of existing commercial processes if they are to be implemented, and their volumes should be such that their utilization in new commercial applications does not significantly impact current utilization needs. Second, as these feedstocks contain in many cases alternate chemical architectures and functionality, product/application development will be needed to identify key properties and commercial product opportunities for these new materials. Finally, new chemical and, in particular, catalytic technologies will need to be developed to transform these feedstocks into useful monomers and materials. Without parallel development on all three of these fronts, commercial implementation will be significantly hindered. Natural seed oil based raw materials meet several of the needs of renewable materials. Their competitive cost, worldwide availability, and built-in functionality make them attractive for numerous commercial applications, and they have already found limited application in several areas, including cosmetics, soaps, detergents, polymer additives, and coatings.[3]

Olefin metathesis of seed oils and their fatty acid methyl esters has been an active area of research for greater than 25 years, with the breakthrough discovery by Mol that supported Re catalysts, activated with tetraalkyltin species, are active in the homometathesis of methyl oleate.[4] This advance led to considerable activity in the development of heterogeneous metathesis catalysts focusing on new catalytic materials, improved activators, and fundamental surface science studies to understand the nature of the catalytically active site.[5,6] However, to date, the highest reported catalyst turnovers for the metathesis of methyl oleate with these heterogeneous catalysts is 900, due to severe catalyst sensitivity to polar impurities and polar functionality and inherently rapid deactivation pathways.[7]

Over the past decade, the ground-breaking research of Schrock,[8−10] Grubbs,[11−17] Hoveyda,[18,19] Herrmann,[20,21]

* To whom correspondence should be addressed. E-mail: brmaughon@dow.com.

(1) Carraher, C. A.; Sperling, L. H. *Polymer Applications of Renewable Materials*; Plenum: New York, 1983.
(2) MacGregor, E. A.; Greenwood, C. T. *Polymers in Nature*; Wiley: New York, 1980.
(3) Gunstone, F. *Inform* **2000**, *11*, 599.
(4) Verkuijlen, E.; Kapteijn, F.; Mol, J. C.; Boelhouwer, C. *J. Chem. Soc., Chem. Commun.* **1977**, 198.
(5) Sibeijn, M.; Poels, E. K.; Bliek, A.; Moulijn, J. A. *J. Am. Oil Chem. Soc.* **1994**, *71*, 553.
(6) Mol, J. C. *Green Chem.* **2002**, *4*, 5.
(7) Chabanas, M.; Coperet, C.; Basset, J.-M. *Chem.- Eur. J.* **2003**, *9*(4), 971−975.
(8) Schrock, R. R.; Depue, R. T.; Feldman, J.; Yap, K. B.; Yang, D. C.; Davis, W. M.; Park, L. Y.; Dimare, M.; Schofield, M.; Anhaus, J.; Walborsky, E.; Evitt, E.; Kruger, C.; Betz, P. *Organometallics* **1990**, *9*, 2262.
(9) Schrock, R. R.; Murdzek, J. S.; Bazan, G. C.; Robbins, J.; Dimare, M.; O'Regan, M. *J. Am. Chem. Soc.* **1990**, *112*, 3875.

10.1021/om0341799 CCC: $27.50 
Publication on Web 03/26/2004

**Scheme 1**

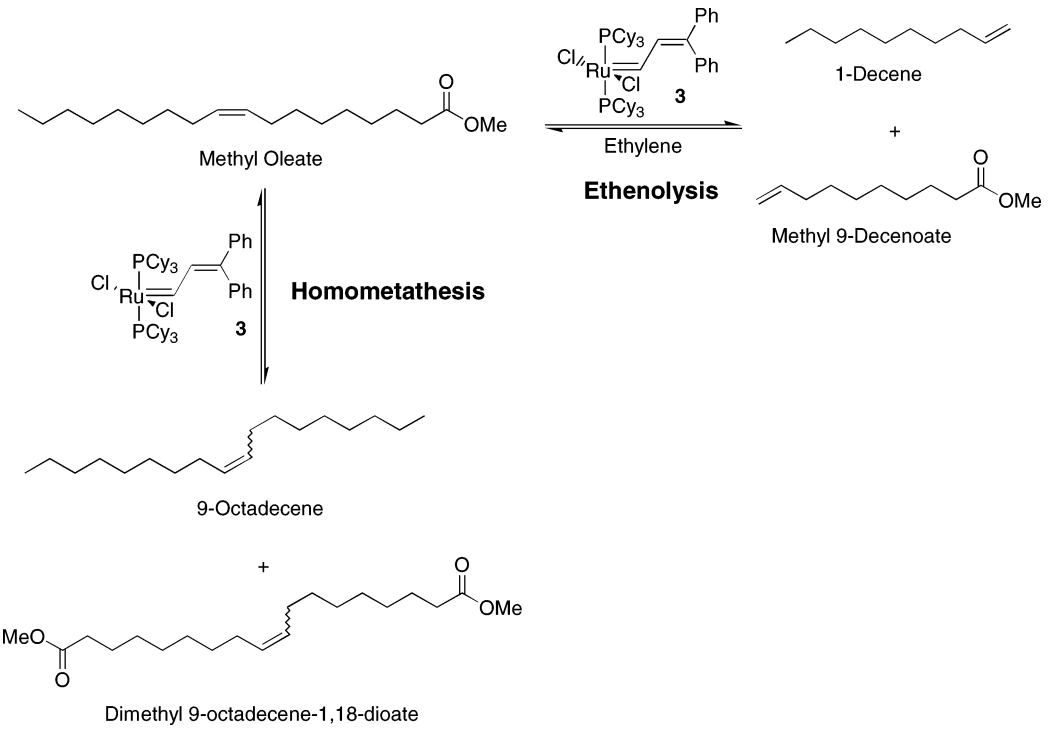


Nolan,[22] and others[23−31] on the development of functional group tolerant homogeneous metathesis catalysts has led to renewed interest in olefin metathesis and its potential in commercial applications.[10,11,32,33] In particular, the first-[12−14] and second-generation[16] Grubbs catalysts, illustrated in Chart 1 (**1** and **2**, respectively),

**Chart 1**

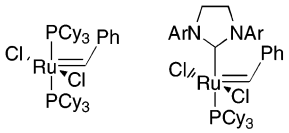

**1** **2**

have received widespread attention due to their tolerance of air, moisture, and a wide array of polar functional groups. This, coupled with their considerable activity and relative ease of synthesis, has led to their evaluation in numerous areas in polymer synthesis[33,34] and organic transformations.[33,35,36] The application of these systems for the metathesis of fatty acid methyl esters has received limited attention, though. In 1994, Grubbs et al. demonstrated that both the homometathesis of methyl oleate (Scheme 1) and its cross-metathesis with ethylene (ethenolysis, Scheme 1) could be accomplished using **3**, giving productive turnovers of 960 and 130−140, respectively, for these reactions.[37] In 2001, Warwel et al. demonstrated turnovers of 2320−2960 for the ethenolysis of methyl oleate at 50 °C/140 psig using **1**.[38] To date, these are the best reported turnovers for the ethenolysis of methyl oleate using homogeneous ruthenium metathesis catalysts. Mol has reported that turnovers of 2500 using **1** and 440 000 using **2** could be achieved for the homometathesis of methyl oleate as well.[39]

With its focus on sustainable development and on the need for the identification of alternate feedstocks, The



(10) Schrock, R. R. *Acc. Chem. Res.* **1990**, *23*, 158.
(11) Grubbs, R. H.; Tumas, W. *Science* **1989**, *243*, 907.
(12) Nguyen, S. T.; Johnson, L. K.; Grubbs, R. H. *J. Am. Chem. Soc.* **1992**, *114*, 3974.
(13) Nguyen, S. T.; Grubbs, R. H.; Ziller, J. W. *J. Am. Chem. Soc.* **1993**, *115*, 9858.
(14) Schwab, P.; Grubbs, R. H.; Ziller, J. W. *J. Am. Chem. Soc.* **1996**, *118*, 100.
(15) Dias, E. L.; Nguyen, S. T.; Grubbs, R. H. *J. Am. Chem. Soc.* **1997**, *119*, 3887.
(16) Scholl, M.; Ding, S.; Lee, C. W.; Grubbs, R. H. *Org. Lett.* **1999**, *1*, 953.
(17) Sanford, M. S.; Love, J. A.; Grubbs, R. H. *J. Am. Chem. Soc.* **2001**, *123*, 6543.
(18) Kingsbury, J. S.; Harrity, J. P. A.; Bonitatebus, P. J.; Hoveyda, A. H. *J. Am. Chem. Soc.* **1999**, *121*, 791.
(19) Garber, S. B.; Kingsbury, J. S.; Gray, B. L.; Hoveyda, A. H. *J. Am. Chem. Soc.* **2000**, *122*, 8168.
(20) Weskamp, T.; Schattenmann, W. C.; Spiegler, M.; Herrmann, W. A. *Angew. Chem., Int. Ed.* **1998**, *37*, 2490.
(21) Weskamp, T.; Kohl, F. J.; Herrmann, W. A. *J. Organomet. Chem.* **1999**, *582*, 362.
(22) Huang, J.; Stevens, E. D.; Nolan, S. P.; Peterson, J. L. *J. Am. Chem. Soc.* **1999**, *121*, 2674.
(23) Gessler, S.; Randl, S.; Blechert, S. *Tetrahedron Lett.* **2000**, *41*, 9973.
(24) Amoroso, D.; Fogg, D. E. *Macromolecules* **2000**, *33*, 2815.
(25) Nieczypor, P.; van Leeuwen, P. W. N. M.; Mol, J. C.; Lutz, M.; Spek, A. L. *J. Organomet. Chem.* **2001**, *625*, 58.
(26) Buchowicz, W.; Ingold, F.; Mol, J. C.; Lutz, M.; Spek, A. L. *Chem. Eur. J.* **2001**, *7*, 2842.
(27) Coalter, J. N.; Caulton, K. G. *New J. Chem.* **2001**, *25*, 679.
(28) Werner, H.; Jung, S.; Gonzalez-Herrero, P.; Ilg, K.; Wolf, J. *Eur. J. Inorg. Chem.* **2001**, 1957.
(29) Stuer, W.; Wolf, J.; Werner, H. *J. Organomet. Chem.* **2002**, *641*, 203.
(30) Wakamatsu, H.; Blechert, S. *Angew. Chem., Int. Ed.* **2002**, *41*, 794.
(31) Connon, S. J.; Rivard, M.; Zaja, M.; Blechert, S. *Adv. Synth. Catal.* **2003**, *345*, 572.
(32) Ivin, K. J.; Mol, J. C. *Olefin Metathesis and Metathesis Polymerization*; Academic Press: San Diego, CA, 1997.
(33) Rouhi, A. M. *Chem. Eng. News* **2002**, *80*(51), 29.
(34) Buchmeiser, M. R. *Chem. Rev.* **2000**, *100*, 1565.
(35) Grubbs, R. H.; Miller, S. J.; Fu, G. C. *Acc. Chem. Res.* **1995**, *28*, 446.
(36) Grubbs, R. H.; Chang, S. *Tetrahedron* **1998**, *54*, 4413.
(37) Grubbs, R. H.; Nguyen, S. T.; Johnson, L. K.; Hillmyer, M. S.; Fu, G. C. WO 9604289, 1996.
(38) Warwel, S.; Bruse, F.; Demes, C.; Kunz, M.; Klaas, M. R. *Chemosphere* **2001**, 39.
(39) Dinger, M. B.; Mol, J. C. *Adv. Synth. Catal.* **2002**, *344*, 671.

Dow Chemical Company has been involved in the exploration of seed oils as a potential raw material for a number of applications in epoxy thermoplastics and thermosets, polyurethane foams, thermoplastic polyurethanes, polyolefin comonomers, and surfactants. The development of olefin metathesis catalysis for the ethenolysis of methyl oleate has been identified as critical to conversion of seed oil based feedstocks into useful raw materials for these application areas. However, the cost of the homogeneous metathesis catalysts requires turnovers of >50 000 in order to achieve an economically viable process. A concerted research effort focusing on experimental reaction and process parameter evaluation, kinetic modeling, and molecular modeling has been undertaken to evaluate catalyst **1** for the ethenolysis of methyl oleate. The goals of this effort are a detailed understanding of the reaction pathways and the factors which impact catalyst performance and the identification of a commercially viable metathesis process.

## Experimental Section

**Materials.** Bis(tricyclohexylphosphine)benzylidine ruthenium dichloride (**1**) was obtained from Strem Chemicals and used without further purification. Methyl oleate (99%) and 1-decene (94%) were obtained from Aldrich and were purified by alumina treatment prior to use. Toluene and $C_6D_6$ were obtained from Aldrich and purified using a fixed-bed purification system.[40] Ethylene (Matheson, polymer grade) was used without purification. 9-Octadecene (97%) was purchased from Alfa Aesar and was purified by alumina treatment prior to use. $Ph_3PO$ was purchased from Aldrich and used without further purification. Methyl 9-decenoate was isolated from the metathesis reaction mixture via distillation and further purified by alumina treatment prior to use.

**Ethylene Solubility Studies.** A Whitey gas cylinder was fitted with a pressure gauge, two shut-off valves, and tubing to connect to the 2 L reactor inlet valve. The volume of the cylinder, valves, and gauge ($V_c$) was determined by filling with methanol and measuring the volume. The volume of all the ports in the top of the Parr reactor was also measured by methanol filling, along with the reactor containing the magnetic stirrer. The sum of the reactor volume, the connecting tubing, and the port volume ($V_r$) was used as the volume into which a known volume of gas was allowed to expand. The reactor was loaded with a known amount of methyl oleate, evacuated for ~10 min at full vacuum, and sealed. The ethylene-purged cylinder and the connecting tubing were secured to the reactor. The Whitey cylinder was filled with ethylene to 128 psig. The fill valve was closed, and the valve to the connecting line and the reactor isolation valve were opened, allowing the known volume of gas to expand into the reactor with vigorous stirring. The cylinder valve was closed, and the cylinder was refilled to 128 psig. This second volume of gas was also allowed to expand into the stirred reactor. This procedure was continued until the reactor pressure read a stable 60 psig for 5 min. The same procedure was used to generate data at 40, 60, 72, and 80 psig. The solubility of ethylene in methyl oleate at various pressures was then calculated.[41] At 60 psig, this corresponded to a mole fraction of ethylene/methyl oleate of 0.108. A similar experiment in which the methyl oleate was saturated with air or nitrogen at the start did not give a good correlation.

**Methyl Elaidate (*trans*-Methyl Oleate) Synthesis.** Elaidic acid (51 g, 0.18 mol) was charged to a 100 mL round-bottom flask along with methanol (20 mL) and 2,2-dimethoxypropane (5.5 mL, 0.045 mol). Approximately 8 drops of sulfuric acid were added, and the solution was refluxed for 30 min. The cooled reaction mixture was poured into 100 mL of 5% sodium bicarbonate containing 200 g of crushed ice. After the ice melted, the mixture was extracted three times with 50 mL portions of diethyl ether. The ether layer was dried over sodium sulfate and concentrated to yield 51.8 g (96.7% yield) of the crude ester. The crude ester was distilled prior to use.

**Metathesis Batch Reaction Procedure.** In a drybox, alumina-treated and degassed Aldrich methyl oleate (12.0 g, 40.47 mmol) and tetradecane (2.5 g, internal standard) were combined with a stir bar in a heavy-walled glass reactor (Ace #8648-135), and this was capped with a rubber septum. Bis(tricyclohexylphosphine)benzylideneruthenium dichloride (**1**; 1.85 mg, 0.002 25 mmol) was then dissolved in toluene (100 $\mu$L) in a gastight syringe, and both the reactor and syringe were removed from the glovebox. The catalyst solution was added in one portion to the reactor, and then the reactor was connected to an ethylene/nitrogen dual manifold and a magnetic stirrer. The reactor was flushed with 2 × 55 psig nitrogen and 1 × 60 psig ethylene, and then it was pressurized up to 60 psig of dynamic ethylene pressure. The reaction was monitored by sampling at reaction pressure via a ETFE shut-off valve through a 0.01 in. i.d. TEFZEL tube inserted into the reaction mixture. The sample was quenched under pressure with excess butyl vinyl ether. Conversion and selectivity were determined using GC analysis on a Hewlett-Packard 6890 instrument using a BPX70 column (60 m × 0.32 mm × 0.2 $\mu$m film thickness; Phenomenex #054617). Samples of the quenched liquid phase (~100 $\mu$L) were diluted in acetone (1.5 mL) before injection. An inlet temperature of 275 °C and detector temperature of 325 °C were used with the following temperature ramp: temperature 1, 80 °C; hold 1, 4 min; ramp 1, 50 °C/min; temperature 2, 170 °C; hold 2, 3 min; ramp 2, 5 °C/min; temperature 3, 200 °C; hold 3, 3 min; ramp 3, 25 °C/min; temperature 4, 255 °C; hold 4, 15 min.

Homometathesis experiments, catalyst loading studies, ethylene pressure experiments (15−60 psig), and reverse coupling reactions of terminal olefins were run similarly in this reactor system.

**High-Pressure Batch Reactor Procedure.** The clean 1 in. stainless steel tubular reactor containing a magnetic Star Head stirring bar was evacuated for 30 min, sealed, and transferred to the drybox. Into a glass vial was weighed tetradecane (2.5 g, internal standard) and Aldrich methyl oleate (12.0 g) that had been degassed and alumina-treated. The reagents were mixed and transferred to the tubular reactor through a piece of plastic tubing entering through the top $^1/_4$ in. fitting and extending to within $^1/_2$ in. of the bottom of the reactor. The top valve on the reactor was closed and capped. A gastight syringe was loaded with a freshly prepared solution of **1** in toluene (0.21 mL of a 0.04 M solution). The sealed reactor and the capped syringe were taken to the reaction manifold. The $^1/_4$ in. fitting was attached to the manifold, and the manifold was purged with 50 psig of nitrogen. The reactor isolation valve was opened, the stirrer was started, and the reactor was flushed 4 × 240 psig with polymerization grade ethylene via a fast-feed valve. The pressure was let down to <5 psig and the catalyst solution injected through the septum port (12 in. needle to reach the reactor contents) on the reactor. The injection port valve was closed and the pressure taken to 240 psig of ethylene with the fast-feed valve. That valve was then closed, and the valve through the mass flow controller was opened for the remainder of the reaction. Samples were taken via the sample loop with a standard purge/sample sequence into a capped GC vial containing ~100 $\mu$L of butyl vinyl ether. The same GC analysis as above was utilized to determine conversion and selectivity.

**$^{31}$P NMR Catalyst Decomposition Experiments.** In the glovebox, a solution of either methyl oleate (0.10 g, 0.34 mmol,

(40) Panborn, A. B.; Giaradello, M. A.; Grubbs, R. H.; Rosen, R. K.; Timmers, F. J. *Organometallics* **1996**, *15*, 1518.
(41) See the Supporting Information.

55.5 equiv) or 1-decene (0.043 g, 0.31 mmol, 50.6 equiv), $Ph_3PO$ (1.7 mg, 0.006 mmol, 1.0 equiv) and **1** (5.0 mg, 0.006 mmol, 1.0 equiv) in $C_6D_6$ was prepared and transferred to an NMR tube, which was capped and sealed with Parafilm. $^{31}P$ NMR spectra were recorded periodically for up to 24 h using a Varian Mercury Vx 300 spectrometer (300.1 MHz; 75.49 MHz for $^{13}C$) using an Sun Ultra 5 workstation running Solaris 7 and VNMR 6.1B software with reference to a $H_3PO_4$ external standard. Integration of the observed ruthenium carbene signals (benzylidene, 37.2 ppm; alkylidene, 36.6 ppm; methylidene, 43.8 ppm) versus the $Ph_3PO$ internal standard (25.65 ppm) was used to determine the concentrations of the different catalyst intermediates over time.

**Kinetic Modeling Studies.** The batch experiments were simulated mathematically by setting up differential equations to account for the material balance for each component in the reaction mixture. The batch simulations were initiated by the initial charge compositions reported for the experimental runs. The predicted profiles for various components were brought into agreement with the experimental data by manipulating the fitting parameters in the postulated kinetic model. The system equations were integrated by using Gear's backward differentiation formula. The Marquardt optimization method was employed for data fitting.

**Computational Studies.** The computational methods employed to compute molecular structures and energetics are based on density functional theory (DFT), as embodied in the Jaguar 4.1 program by Schrodinger, Inc.[42] The B3LYP hybrid functional and the LACVP** basis set were used to describe the electronic structure. LACVP** comprises the Los Alamos effective core potential on the Ru atom and the 6-31G** basis set on all non-transition-metal elements. All geometries were optimized using the Jaguar 4.1 built-in optimizer until the maximum gradient of the energy with respect to nuclear displacement was smaller than $10^{-3}$ atomic units. If this residual gradient was not reached during the optimization, the optimization was examined and accepted only if all quality criteria (except for the maximum gradient) had been met. Conformational searches were done with the conformational search module of Cerius[2], using the UFF force field, with subsequent local optimization. For conformations involving organometallic bonds, a limited conformer search was done at the Jaguar 4/DFT level of theory. Transition states were located by geometry scans of the C−C bond length in increments of 0.2 Å, which is sufficient to determine the transition state energy to within 0.5 kJ/mol, due to the flatness of the potential energy surface in the region of the transition state. All computed energies reported here are pure density functional energies.



## Results and Discussion

**Preliminary Laboratory Studies.** Initially, simple probe metathesis reactions were carried out for the ethenolysis of methyl oleate, using **1** in batch reactors to begin to understand the impact of standard process variables on this cross-metathesis reaction. Figure 1 illustrates the ethenolysis of neat methyl oleate using **1** at room temperature/60 psig of ethylene with [MO]/[**1**] = 4500:1. Under these mild conditions, several reaction features are apparent. First, high selectivity to the desired terminal olefin products (1-decene and methyl 9-decenoate) is apparent at low conversions, but this selectivity decreases with increasing conversion. Second, a high initial rate is observed (1.4 TO/s) that rapidly decreases during the first 2 h of reaction. The high initial rate and substantial turnovers (TO = 2980)

(42) Jaguar 4.0; Schrodinger, Inc., Portland, OR, 2000.

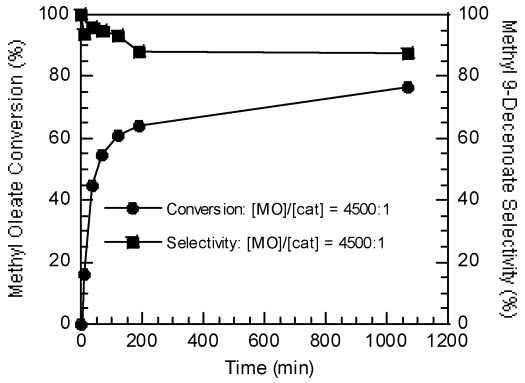


**Figure 1.** Conversion of methyl oleate (MO) in the MO ethenolysis with catalyst **1**. Conditions: 30 °C; 60 psig of ethylene; 4500:1 [MO]/[**1**]; [MO] = 2.56 M; 2980 turnovers.

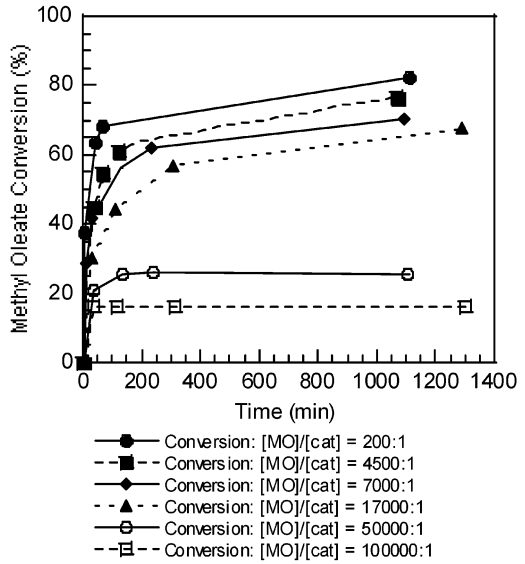


**Figure 2.** Conversion of methyl oleate (MO) in the MO ethenolysis with catalyst **1**. Conditions: 30 °C; 60 psig of ethylene; [MO]/[**1**] ratios of 200, 4500, 7000, 17 000, 50 000, and 100 000; [MO] = 2.56 M.

observed in this reaction under such mild conditions were promising and prompted further exploration. Catalyst turnovers will be discussed frequently through this report, and therefore their definition is worth highlighting as it relates to this chemistry. As the desired products are the terminal olefins 1-decene and methyl 9-decenoate, not the internal olefin isomers of methyl oleate (or the homometathesis products), turnovers will be defined as the productive turnovers to one of the desired terminal olefin products, as illustrated:

$$\text{catalyst turnovers (TO)} = (\text{moles of either 1-decene or methyl 9-decenoate produced})/(\text{mole of catalyst})$$

$$\text{TOF} = \text{initial catalyst turnovers/s}$$

**Catalyst Loading.** To push the limits of this chemistry under these conditions, a series of experiments have been run at a range of catalyst loadings, as shown in Figure 2. Catalyst loadings from 200:1 to 100 000:1 have been studied to determine the impact of catalyst loading on initial activity, selectivity, and total turnovers. Table 1 shows the impact of catalyst loading on both initial TOF and total batch turnovers achieved. Quite remarkably, the initial rates are high even at low

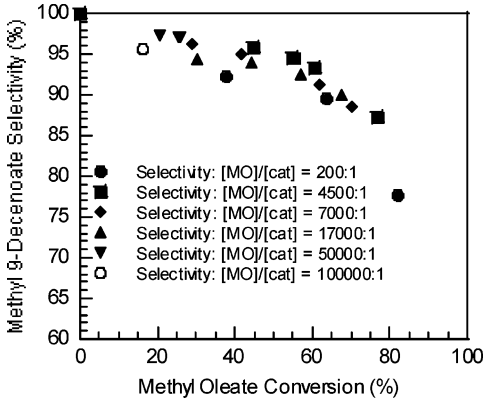


**Figure 3.** Selectivity of methyl oleate (MO) ethenolysis with catalyst **1** versus MO conversion. Conditions: 30 °C; 60 psig of ethylene; [MO]/[**1**] ratios of 200, 4500, 7000, 17 000, 50 000, and 100 000; [MO] = 2.56 M.

**Scheme 2**

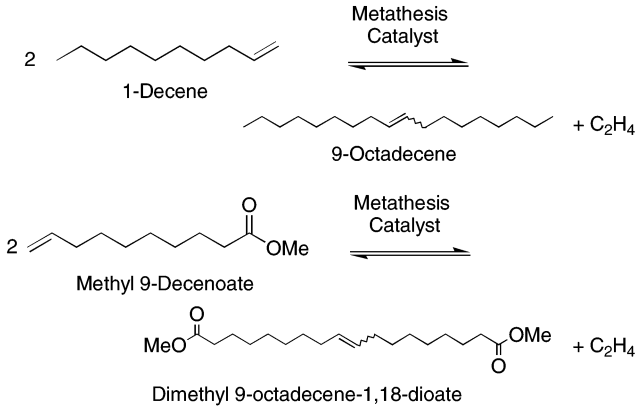


**Table 1. Impact of the Initial Catalyst Loading on Initial TOF's and Total Turnovers**

| [MO]/[cat] ratio | TOF (productive TO/s) | catalyst turnovers |
|---|---|---|
| 200 | 0.05 | 127 |
| 4 500 | 0.9 | 3 010 |
| 7 000 | 1.5 | 4 350 |
| 17 000 | 2.5 | 10 400 |
| 50 000 | 4.8 | 12 500 |
| 100 000 | 6.7 | 15 400 |

catalyst loadings, with initial TOF's up to 6.7/s and total turnovers of >15 000 achievable under these conditions.

If the selectivity to terminal olefin products is plotted versus methyl oleate conversion, a clear trend is observed for all of these loadings. As can be seen in Figure 3, the selectivity to terminal olefin products is typically >94% at conversions of <50%, but as the conversions increase past this point, the selectivity rapidly decreases due to the increased contribution of the terminal olefin self-metathesis reaction seen in Scheme 2. Therefore, catalyst **1** initially gives a kinetic product mixture favoring terminal olefin products (1-decene and methyl 9-decenoate), but this then trends toward the thermodynamic product mixture, where higher levels of internal olefins (9-octadecene and dimethyl 9-octadecene-1,18-dioate) are formed over extended reaction times and conversions.

**Ethylene Pressure.** To attempt to drive the cross-metathesis of methyl oleate and ethylene to higher conversions and selectivities, the impact of ethylene pressure has been examined. Standard conditions of

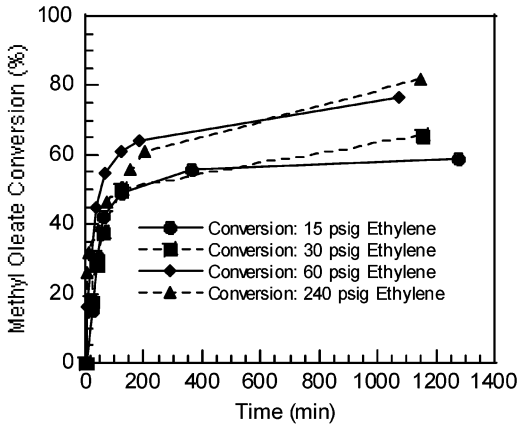


**Figure 4.** Conversion of methyl oleate (MO) in the MO ethenolysis with catalyst **1**. Conditions: 30 °C; ethylene pressures of 15, 30, 60, and 240 psig; 4500:1 [MO]/[**1**]; [MO] = 2.33 M.

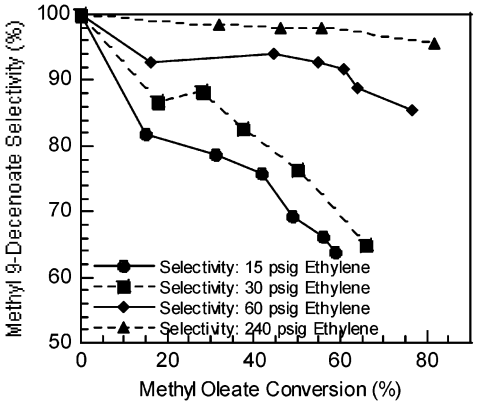


**Figure 5.** Selectivity of methyl oleate (MO) ethenolysis with catalyst **1** versus MO conversion. Conditions: 30 °C; ethylene pressures of 15, 30, 60, and 240 psig; 4500:1 [MO]/[**1**]; [MO] = 2.33 M.

[MO]/[**1**] = 4500:1 at room temperature have been employed with ethylene pressures from 15 to 240 psig. Figure 4 illustrates the conversion profiles at these pressures. Although the conversion is found to increase from 56% to 82% on going from 15 to 240 psig, surprisingly, the initial rates for these different pressure experiments are not significantly different, implying that the rate dependence on ethylene concentration is not first order. However, as expected, the selectivity is significantly affected by ethylene pressure, with selectivities of >96% possible at 240 psig, even at high conversion (Figure 5).

**Cis/Trans Equilibration.** One issue of concern is that as this reaction proceeds, equilibration of the internal olefins (methyl oleate, 9-octadecene, and dimethyl 9-octadecene-1,18-dioate) to a cis/trans mixture is expected. As the reaction starts with >99% *cis*-methyl oleate, the impact that the formation of trans internal olefins in the reaction mixture would have on catalyst productivity was not clear. The concentrations of cis/trans olefins are illustrated in Figure 6 for the ethenolysis of methyl oleate using **1** at 30 °C/60 psig of ethylene and [methyl oleate]/[**1**] = 4500:1. For clarity, only methyl 9-decenoate, methyl oleate, and dimethyl 1,18-octadec-9-enedioate values are shown.

From this, one can see that, with catalyst **1**, low levels of trans olefin do grow in with time, and for the

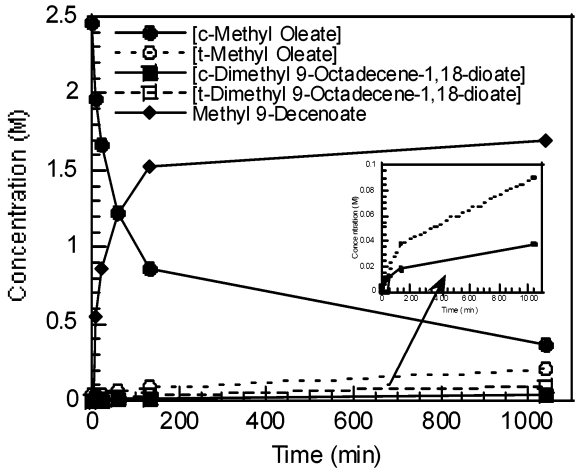


**Figure 6.** Concentration profiles of selected reactants and products (including cis/trans isomers) in the MO ethenolysis with catalyst **1**. Conditions: 30 °C; 60 psig of ethylene; 4500:1 [MO]/[**1**]; [MO] = 2.56 M; 2980 turnovers.

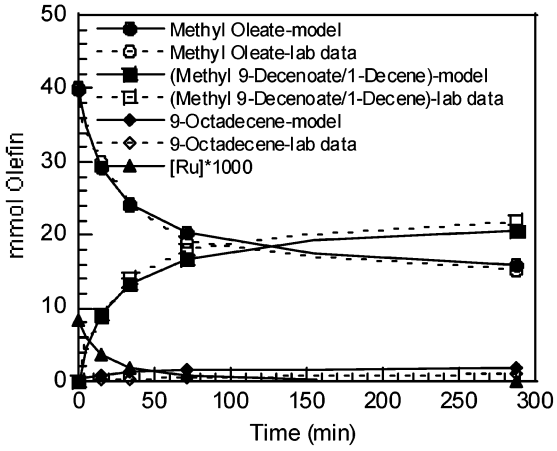


**Figure 7.** Comparison of experimental data versus the second-order reversible model for MO ethenolysis with catalyst **1**. Conditions: 30 °C; 60 psig of ethylene; 4500:1 [MO]/[**1**]; [MO] = 2.56 M; 2980 turnovers.

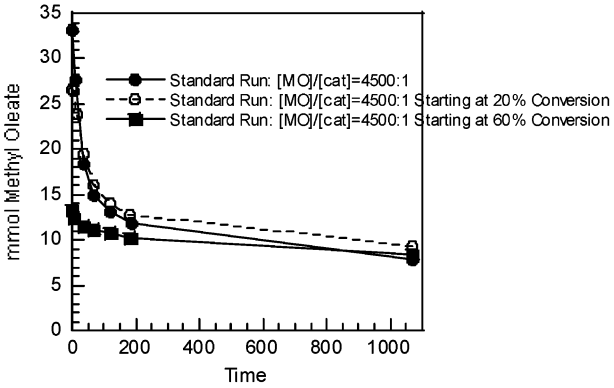


**Figure 8.** Effect of product addition on the rate of methyl oleate (MO) conversion in the MO ethenolysis with catalyst **1**. Conditions: 30 °C; 60 psig of ethylene; [**1**] = 0.57 mM; for the standard run, [MO] = 2.561 M; starting at 22% conversion, [MO] = 1.92 M, [1-decene] = 0.48 M, [methyl 9-decenoate] = 0.52 M, [9-octadecene] = 0.020 M; starting at 60% conversion, [MO] = 0.80 M, [1-decene] = 1.18 M, [methyl 9-decenoate] = 1.21 M; [9-octadecene] = 0.077 M.

homometathesis byproducts, trans olefin dominates the cis species by a 2.4:1 ratio. However, these results show that neither homometathesis nor trans olefin formation are kinetically significant relative to methyl oleate ethenolysis.[43]

**Kinetic Modeling Studies. A. Semiempirical Kinetic Modeling.** With these basic screening experiments in hand, an extensive data analysis effort was initiated in order to better understand the complex phenomena governing the methyl oleate ethenolysis. As expected, it was concluded that a simple kinetic fit based on a second-order reversible model (see eq 1) fails to fit the experimental results.

$$\text{methyl oleate} + \text{ethylene} \underset{k_2}{\overset{k_1}{\rightleftharpoons}} \text{1-decene} + \text{methyl 9-decenoate} \quad (1)$$

The key reason is the presence of an unusual slowdown of conversion in every batch experiment, following a rapid initial rate, which could not be explained simply by the adverse effect of the accelerating reverse reaction. Mathematically, this unexpected reactivity loss could only be accounted for by employing a rapid second-order catalyst decay. Both the fit to the experimental data and the predicted catalyst decay profile using empirical second-order catalyst decay are seen in Figure 7. *The apparent catalyst half-life of near 10 min necessary to fit the experimental data is in conflict, however, with previous reported ruthenium methylidene and alkylidene half-lives of 40 min and 8 h at 55 °C, respectively.*[44] These literature decay studies have been accomplished in the absence of olefinic substrates, and therefore one cannot assume that they directly translate to our system, but the significant discrepancy prompted us to explore the framework of the kinetic model in a more detailed fashion.

The simple reversible model (eq 1) also failed to explain and fit a number of experimental runs in which catalyst loading was varied. It is readily observed in Figure 2 that the experimentally attainable apparent equilibrium conversion is systematically related to the catalyst concentration. That is, the lower the catalyst concentration, the lower the observed plateau in conversion. Also, regarding the ethylene pressure effect (Figure 4), complex phenomena were again observed instead of the expected first-order behavior, which the simple model failed to explain.

The experiments with the presence of the products in the initial charge provided invaluable insight. In Figure 8, the methyl oleate decay profiles for two batch runs containing products in the initial charge, simulating partially converged methyl oleate at 20 and 60% conversion, were compared with a similar run starting with only methyl oleate. The run conditions were identical at 30 °C and under 60 psig ethylene pressure. In particular, it should be mentioned that all three

(43) The rate of both homometathesis and ethenolysis of methyl oleate has therefore been examined by comparing the cis and trans olefin isomers (Figures 24 and 25 in the Appendix). Clearly, the rate of trans olefin metathesis is considerably lower than that of cis olefin, for both homometathesis and ethenolysis, similar to previous reports.[48] During a typical batch experiment only low levels of trans olefin are observed, and therefore, this impact of catalyst activity should be minimal. This effect will need to be considered in future process studies, though, as trans olefin will build up on recycling of the metathesis mixture and thus could impact catalyst performance to a greater degree.

(44) Ulman, M. U.; Grubbs, R. H. *J. Org. Chem.* **1999**, *64*, 7202.

experiments employed fresh catalyst with identical concentrations.

A close comparison of the methyl oleate decay profiles in Figure 8 qualitatively indicates that the batch run starting with a charge corresponding to 20% conversion behaves very similarly to the control run following 20% conversion. Therefore, one can conclude that, at least up to 20% conversion, the catalyst degradation is not significant. Please note that the control run starts with methyl oleate, without the presence of the products, and as the conversion rises the products continue to build up. Therefore, the only difference between the control run at 20% conversion and the batch run starting with a mixture corresponding to 20% conversion is the used catalyst versus the fresh catalyst.

Similarly, in the batch run starting with an initial charge corresponding to 60% conversion, the methyl oleate decay appears to begin with a somewhat faster, but comparable, rate to the control run following 60% conversion. *This observation clearly indicates that there is an adverse effect of the terminal olefin product on the reactivity and that significant catalyst decay in the control run cannot be the sole cause of catalyst activity losses at higher conversion.* Fitting these experiments using the simple reversible model was unsuccessful.

To investigate the role of the terminal olefin products on the catalyst activity and the complex role of ethylene pressure and the catalyst loading, a more detailed mechanistic-based kinetic discussion follows.

**B. Mechanistic-Based Kinetic Discussion for Olefin Cross-Metathesis.** It should be emphasized that a comprehensive list of the elementary reactions involved in methyl oleate ethenolysis includes numerous individual reactions (see Computation Studies). This is due to the presence of many productive and nonproductive reactions of various catalytic intermediates as well as the presence of a large number of the cis/trans isomers in the mixtures contributing to the reaction system. Furthermore, in addition to the reversible reactions of various olefins with ruthenium intermediates, there are irreversible reactions responsible for the catalyst decay phenomena. Therefore, to develop a manageable kinetic model, there is a challenge in identifying key reactions, ignoring kinetically noncompetitive ones, and lumping as many steps together as possible while still satisfying the overall equilibrium phenomena. Considering only the net reaction

$$(PCy_3)_2Ru{=}CHR_1 + R_2HC{=}CR_3 \rightleftharpoons (PCy_3)_2Ru{=}CHR_2 + R_1HC{=}CHR_3$$

with $R_1$, $R_2$, and $R_3$ being $(CH_2)_7CH_3$, $(CH_2)_7COOMe$ (16e ruthenium alkylidenes **4** and **5**, respectively) and H (16e ruthenium methylidenes **6**), one can express the majority of metathesis reactions occurring in the reaction mixture by six equations in Schemes 3−5.

On the basis of previous reported studies on catalyst decay of ruthenium alkylidene and methylidene intermediates **4**−**6**, contribution of the **4** and **5** decay rates to the overall catalyst decomposition rate should be minimal.[44] Therefore, loss of catalyst can be attributed predominantly to the decay of **6**, which has been determined to follow first-order decay kinetics (Scheme 6).[44]

**Scheme 3. Methyl Oleate Reaction with 6**

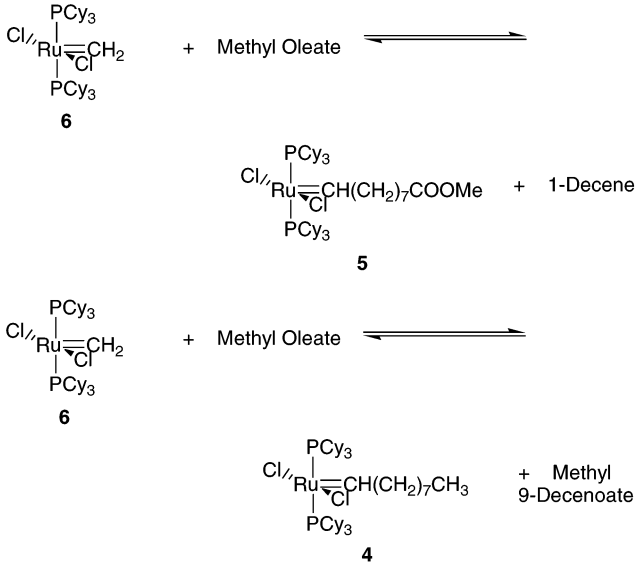


**Scheme 4. Homometathesis Product Reactions with 6**

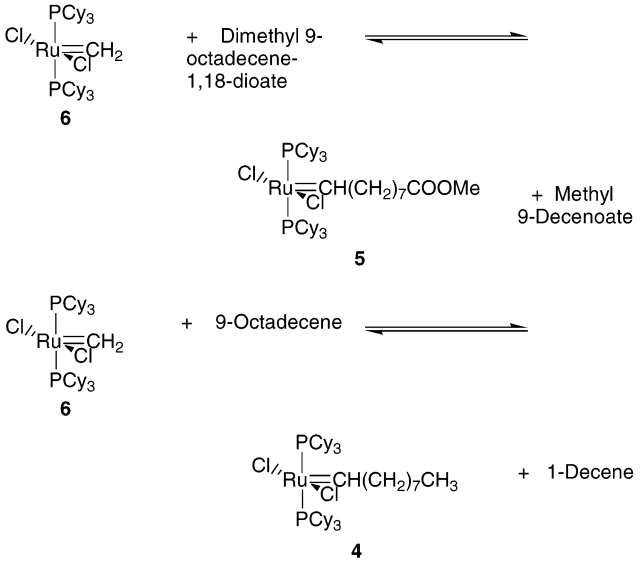


It should be noted that, as mentioned above, these reactions do not completely cover all potential reaction pathways; duplicate reactions involving cis/trans internal olefin would need to be included in addition to the alkyl exchange reactions between the Ru−alkylidene species **4** and **5** and internal olefins. Also, separate ligand dissociation, $\pi$-complexation, and metallacycle formation/cleavage steps would need to be included.[15,17,45,46] A fully expanded version of these reactions, including these elementary steps, is shown in Scheme 7 and will be explained in greater detail in Computational Studies. However, the additional number of fitting parameters that this would contribute would make it impossible to identify a meaningful unique solution to this kinetic model, and therefore a few simplifying assumptions have been employed to develop a workable model for the observed behaviors.

(45) Herrison, J. L.; Chauvin, Y. *Makromol. Chem.* **1970**, *141*, 161.
(46) Sanford, M. S.; Ulman, M.; Grubbs, R. H. *J. Am. Chem. Soc.* **2001**, *123*, 749.

**Scheme 5. Ethylene Reaction with Alkylidenes 4 and 5**

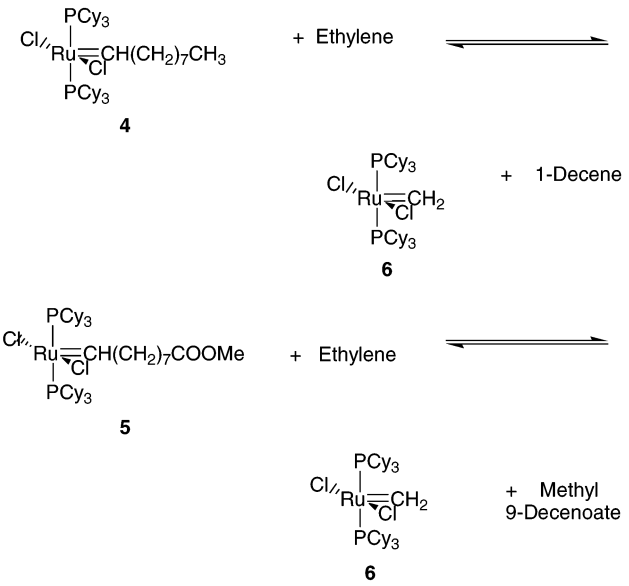


**Scheme 6. Decay of 6**

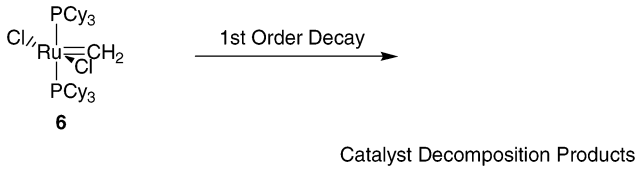


First, the experimental data reveal that although the trans isomers continue to form and accumulate in the course of the batch runs, the concentration of trans olefin is quite low and could therefore be ignored for catalyst **1.** Also, the reaction of **4** or **5** with internal olefins can be excluded, as this reaction is not significant under these conditions with catalyst **1**. The latter approximation is well justified by both homometathesis rate studies with **1** in this report (see Figure 25 in the Appendix) and computational data presented in Computational Studies. The fitting parameters can be further reduced in number with the assumption that the alkyl- and ester-terminated ruthenium alkylidene species **4** and **5** are equally reactive, a reasonable assumption based on the functional group remote proximity relative to the metal center (see Computational Studies) and kinetic studies (see Figure 26 in the Appendix).[47]

To represent the crucial catalyst activation step in which a phosphine ligand is dissociated (Scheme 8) from the 16e ruthenium alkylidene and methylidene intermediates **4**−**6**, the equation (2) for predicting the quasi steady-state concentration of the fourteen-electron ruthenium complexes **7**−**9** was derived for both the alkylidenes **4**/**5** and methylidene intermediates **6**. Therefore, ruthenium methylidene and alkylidene intermediates are incorporated into the kinetic model as coordinated 16e complexes **4**−**6**. The active 14e intermediates (**7**−**9**) which carry out the key catalytic steps are formed from the original 16e ruthenium complex by phosphine dissociation, as shown in Scheme 8. Equation 2, whose basic functional form has also been introduced by others,[17] implies that the equilibration between 16e species and the active 14e species is instantaneous and that the ratio between the concentrations of a given 16e species and its 14e derivative is influenced by competition between phosphine ligand and terminal olefin. In this system, the terminal olefin concentration keeps increasing as the methyl oleate conversion progresses, which may result in further reduction in active 14e complexes. In the semiempirical model it was found that the terminal olefin competitions are dominant. Note that inclusion of terminal olefin complexation as a dominant phenomenon in reducing the concentration of the active ruthenium complex will readily result in a progressive activity retardation in methyl oleate cross-metathesis, consistent with the experimental results.

$$[\text{14e alkylidene } \mathbf{7} \text{ or } \mathbf{8}] \propto \frac{[\mathbf{4} \text{ or } \mathbf{5}]}{[\mathrm{L}] + k'[\mathrm{RCH{=}CH_2}]}$$

$$[\text{14e methylidene } \mathbf{9}] \propto \frac{[\mathbf{6}]}{[\mathrm{L}] + k'[\mathrm{RCH{=}CH_2}]} \quad (2)$$

The denominator of eq 2 represents a competition between the free phosphine ligand (represented by [L]) and terminal olefin for the catalyst open coordination site. One might expect the binding behavior of terminal olefins to depend on the structure of the catalyst species (14e species **7**−**9**). However, in the interest of minimizing the number of fitting parameters, equal complexation characteristics have been assumed. It was also assumed that the free ligand concentration is simply proportional to ruthenium concentration and that the proportionality factor is equal for species **4**−**6**.

Taken together, these outlined assumptions have allowed the generation of a much simpler kinetic model with a manageable number of fitting parameters (see Scheme 9), which was used throughout the present work.

**C. Equilibrium Analysis of Methyl Oleate/Ethylene Metathesis.** The skeleton of the mechanistic model as discussed in the above is made up of two reversible reactions. The first reaction is the methyl oleate (or other internal olefin) reaction with **6** to form a terminal olefin and an alkylidene (**4** or **5**, which are assumed to be equivalent). The second reaction involves the reaction of **4**/**5** with ethylene to form the second terminal olefin product and **6**. A close inspection of the two key reactions reveals that, by combining the two reactions, one generates the overall reversible reaction, representing the stoichiometry of the methyl oleate metathesis with ethylene. Consequently, the two equilibrium constants ($K_1$ and $K_2$), corresponding to the two lumped elementary reactions, would be related as shown in eq 3 to satisfy the overall equilibrium ($K_3$) in the methyl oleate ethenolysis reaction.

$$K_1 K_2 = K_3 \quad (3)$$

Since the overall equilibrium constant ($K_3$) can be estimated experimentally, there is a need to fit for only one of the equilibrium constants. That is, one need only

(47) This assumption has been tested by comparing the rate of terminal olefin coupling with either 1-decene or methyl 9-decenoate, as shown in Figure 26 in the Appendix. The near-identical conversion rates for these two substrates support the postulate of equal reactivity for **4** and **5**.

**Scheme 7**

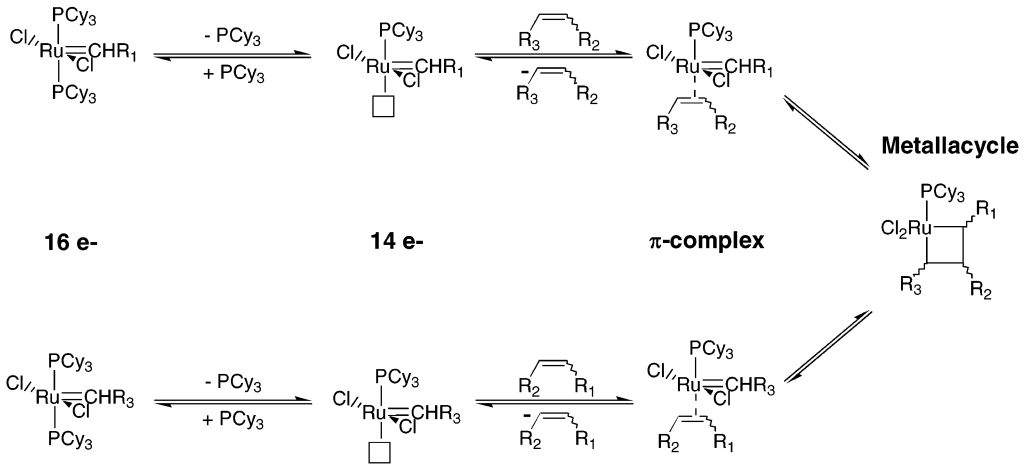


**Scheme 8**

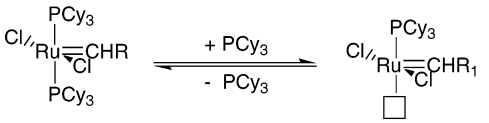

**6**: R =H
**5**: R=$(CH_2)_7COOMe$
**4**: R= $(CH_2)_7CH_3$

**9**: R =H
**8**: R=$(CH_2)_7COOMe$
**7**: R= $(CH_2)_7CH_3$

**Scheme 9**

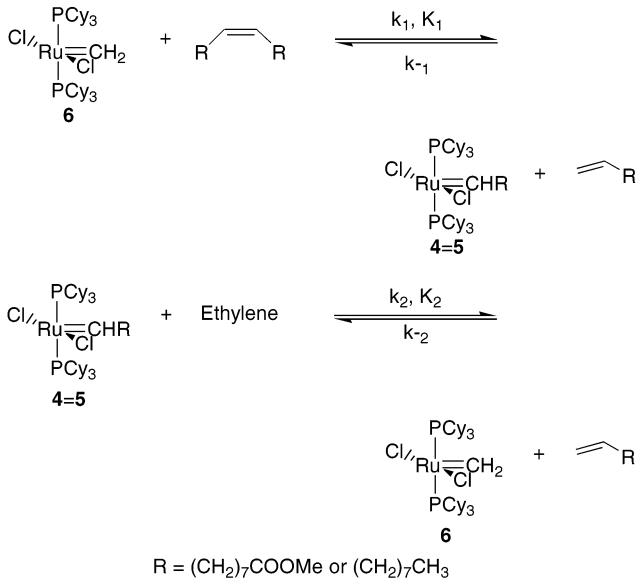


fit for either $K_1$ or $K_2$ if the experimentally derived $K_3$ is utilized to calculate the other constant. The following fundamental analysis has been used to prove the consistency of the experimental data, ensuring the experimental reliability of the equilibrium calculations for $K_3$.

The equilibrium constants of the main and side reactions in methyl oleate ethenolysis are summarized as follows.

Methyl oleate reaction with ethylene (see Scheme 1):

$$K_3 = \frac{k_3}{k_{-3}} = \frac{[\text{methyl 9-decanoate}][\text{1-decene}]}{[\text{methyl oleate}][\text{ethylene}]} \quad (4)$$

**Table 2. Experimental Equilibrium Constants for the Terminal Olefin Self-Metathesis Reactions ($K_5$, $K_6$) and Methyl Oleate Homometathesis ($K_4$)**

| | |
|---|---|
| $K_4$ | 0.25 |
| $K_5$ | 0.03 |
| $K_6$ | 0.03 |

Methyl oleate homometathesis forming 9-octadecene and dimethyl 9-octadecene-1,18-dioate (diester) (see Scheme 1):

$$K_4 = \frac{k_4}{k_{-4}} = \frac{[\text{diester}][\text{9-octadecene}]}{[\text{methyl oleate}]^2} \quad (5)$$

Methyl 9-decenoate self-metathesis reaction to form dimethyl 9-octadecene-1,18-dioate (diester) (see Scheme 2):

$$K_5 = \frac{k_5}{k_{-5}} = \frac{[\text{diester}][\text{ethylene}]}{[\text{methyl 9-decanoate}]^2} \quad (6)$$

1-Decene self-metathesis reaction to form 9-octadecene (see Scheme 2):

$$K_6 = \frac{k_6}{k_{-6}} = \frac{[\text{9-octadecene}][\text{ethylene}]}{[\text{1-decene}]^2} \quad (7)$$

A close examination of the equations for the equilibrium constants presented in above reveals that the four reactions are related according to the equation

$$K_4 = K_2^2 K_5 K_6 \quad (8)$$

In other words, given any three equilibrium constants, the fourth one can be estimated from the above relation. This relation is very valuable, because it can be used to confirm the equilibrium conversions in the experimental data. The equilibrium constants for the side reactions (internal olefin homometathesis and terminal olefin self-metathesis) have been determined experimentally through running each reaction at high catalyst loading to ensure equilibrium is reached, and the results are summarized in Table 2.[41]

Applying the equilibrium relation among the four reactions presented in the above, one can predict the overall equilibrium constant ($K_3$) from the equilibrium

**Table 3. Experimental Equilibrium Constants for Methyl Oleate Ethenolysis Reactions**

| | |
|---|---|
| $K_3$ | 16.47 |
| $K_4$ | 0.22 |
| $K_5$ | 0.03 |
| $K_6$ | 0.03 |

**Table 4. Kinetic Parameter Estimation Using the Kinetic Model**

| | |
|---|---|
| $k_1$ ($min^{-1}$) | 0.0471 |
| $k_{-1}$ ($min^{-1}$) | 0.0880 |
| $k_2$ ($min^{-1}$) | 0.8821 |
| $k_{-2}$ ($min^{-1}$) | 0.0286 |
| $K_1$ | 0.53552 |
| $K_2$ | 30.81 |
| terminal olefin retardation ($k'$) | $1.69 \times 10^{-3}$ |

constants measured for the individual reversible reactions:

$$K_3 = \sqrt{\frac{K_4}{K_5 K_6}} = \sqrt{\frac{0.25}{0.03 \times 0.03}} = 16.7 \qquad (9)$$

This estimate of the equilibrium constant for the main reaction is in good agreement with the corresponding experimental results summarized in Table 3, which were extracted from the methyl oleate ethenolysis reaction accomplished at high catalyst concentration ([MO]/[**1**]) = 200:1 to ensure attainment of equilibrium. Further supporting the use of the equilibrium constants from the experiment at high catalyst loading is the consistency of the measured $K_3$, $K_5$, and $K_6$ values. On the basis of simply a statistical analysis, one would predict that $K_3 = 1/(2K_5)$ or $1/(2K_6)$, and the laboratory values for $K_5$ and $K_6$ lead to a $K_3$ value of $1/(2 \times 0.03) = 16.7$. On the basis of this analysis, the measure of the overall reaction equilibrium constant, $K_3$, appears to be highly reliable.

**D. Kinetic Parameter Estimations.** Using the kinetic model, the experimental data have been simulated mathematically to predict the composition of the reaction mixture over time. The simulations are started by a batch charge corresponding to the initial batch composition run in each experiment, and constant volume is assumed throughout the run. A Henry constant of 220 psia L/mol is used, on the basis of the results from a series of ethylene solubility studies.[41] The profiles of the intermediate components have been evaluated both by exact integration and by using the steady-state assumption, which is a common practice in modeling the concentrations of species which are orders of magnitude smaller than the primary components. Close agreement has been observed for these two methods.

The results from the data fitting are summarized in Table 4. To highlight some of the key observations, the rate of ethylene reaction with the **4**/**5** complex ($k_2$) is the fastest rate in the cycle, as one might expect, while it appears that the reaction of **6** and internal olefin ($k_1$) is the slowest step in the catalytic cycle (see Computational Studies) after phosphine dissociation. These results show that there may be limitations in driving the reaction by increasing the ethylene pressure. In addition, it should mentioned that, due to the possible catalyst inhibition by ethylene, the added benefit of high ethylene pressure diminishes at high pressures.

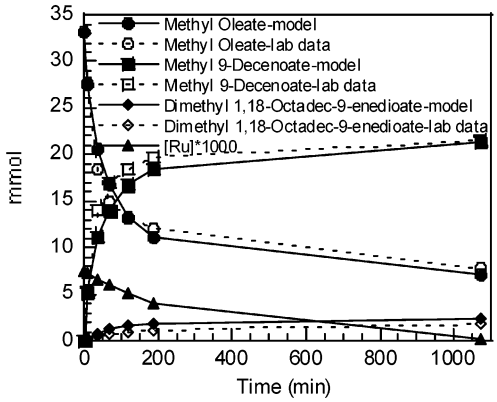


**Figure 9.** Comparison of experimental data and the results from the kinetic model for the concentration profiles of selected reactants and products in the MO ethenolysis with catalyst **1**. Conditions: 30 °C; 60 psig of ethylene; 4500:1 [MO]/[**1**]; [MO] = 2.56 M; 2980 turnovers.

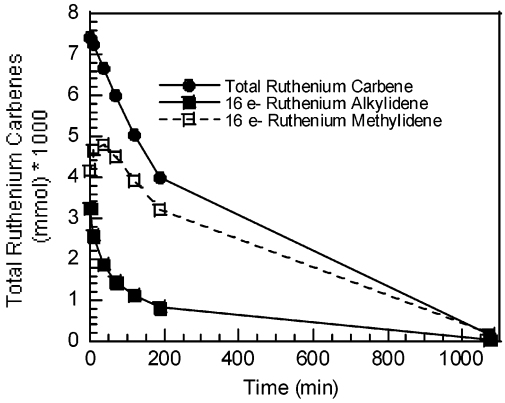


**Figure 10.** Prediction of the concentration profiles of the ruthenium carbene intermediates (**4**/**5** and **6**) in the MO ethenolysis with catalyst **1**. Conditions: 30 °C; 60 psig of ethylene; 4500:1 [MO]/[**1**]; [MO] = 2.56 M.

The comparison of the model fit versus the standard 4500:1 run is demonstrated in Figure 9, showing good consistency with the experimental data. A complete summary of the laboratory data and model fit over a range of conditions can be found in the Supporting Information. One feature of this model is that it allows us to predict the relative change in **6** and **4**/**5** concentrations over the course of the reaction, and this is illustrated in Figure 10, again for our standard 4500:1 run. The buildup of **6** at the expense of **4**/**5** as conversion increases can be easily extrapolated from the kinetic constants. The rate of reaction of terminal olefin and **4**/**5** ($k_{-1}$) is approximately 4× that for the reaction between terminal olefin and **6** ($k_{-2}$), and thus as terminal olefins build up in the reaction mixture, the concentration of **6** rises.

*A key insight one gains from the kinetic model is the fact that there is no solution where the catalyst decay is the sole cause of the observed catalyst activity losses.* Instead, the model readily shows that, in addition to the expected catalyst decay, it is necessary to correlate the formation of terminal olefins with a reduction in catalyst productivity. The addition of terminal olefin to the reaction mixture (see Figure 8) could be expected to lower the reaction rates by competing for the 14e methylidene complex **9** with internal olefin (product inhibition). The inhibition of the catalyst by terminal

olefin product, which presumably occurs by withdrawal of Ru from the "productive" cycle into competing $\pi$-complexes and metallacycles of the terminal olefins (see Computational Studies), has been incorporated semi-empirically as a retardation term into the quasi-steady-state estimation of the concentrations of the active 14e intermediates **7**−**9**. This means that, at higher terminal olefin formation, the concentration of the active intermediates **7**−**9** is lowered and the reaction rate is suppressed. As 2 mol of terminal olefins are formed for every 1 mol of reacted methyl oleate, the impact of terminal olefins on catalyst productivity is significantly enhanced at high conversions.

In addition, the form of eq 2 in the kinetic model predicts the partial conversion plateau as a function of the catalyst loading, which is consistent with our experimental data. The relative concentrations of terminal olefin relative to catalyst dictate the amount of the predicted free 14e complexes **7**−**9**, which are active for metathesis. Thus, at lower catalyst concentrations, product inhibition becomes dominant at correspondingly lower conversions. Again, the primary cause of this terminal olefin retardation has not been conclusively identified, but it presumably occurs primarily by siphoning off active catalyst into competing $\pi$-complexes and metallacycles of the terminal olefins.

Terminal olefins can further impact catalyst productivity by increasing the number of degenerate reaction pathways and by shifting the catalyst intermediates toward higher concentrations of **6** over **4**/**5**. This increase in **6** with increased conversion results in a higher rate of catalyst deactivation coupled with lower catalyst productivity resulting from the concomitant product inhibition. Investigation of other potential roles of terminal olefin in the reduction of catalyst activity are under investigation.

It should be reiterated that in the quasi-steady-state calculation of the concentration of 14e ruthenium complexes, many assumptions have been made. In particular, the complexation of each type of olefin (such as terminal, cis-internal, and trans-internal) with ruthenium is expected to be different. Even more clearly, the methylidene and different alkylidene species are not expected to share the same complexation behavior when interacting with free phosphine and the olefins.[17] These assumptions notwithstanding, this work clearly demonstrates that terminal olefins have a detrimental impact and that the development of processes for either selective product removal to drive the reaction and limit product inhibition or for catalyst removal/recycling will be necessary to improve catalyst efficiency to economically viable levels.

**E. Catalyst Degradation.** As there has been no in situ measure for the rate of catalyst decomposition, the previously measured first-order decomposition rate of **6** has been used in the above model.[44] This rate results in a significantly reduced rate of deactivation with that initially projected in Figure 6, and the rates from these two kinetic models can be compared in Figures 6 and 9. This reported decomposition rate results in an estimated catalyst half-life of 160 min when extrapolated from literature values to room temperature, much closer to that expected from experimental results than early fitting for catalyst decay using a simple second-order reversible model (eq 1). However, one key difference between these experimental results and the previously reported decomposition experiments is that these experiments were carried out in the presence of olefin while doing productive catalyst turnovers, whereas the experiments on the decomposition of the ruthenium methylidene complex were carried out in the absence of olefinic substrates. To the authors' knowledge, no studies on the decomposition of **6** in the presence of olefinic substrates have been accomplished. It is unclear if the rate of decomposition would be comparable in the two cases; therefore, a few further probe studies have been accomplished to gain a better idea of the rate of catalyst decomposition in this system.

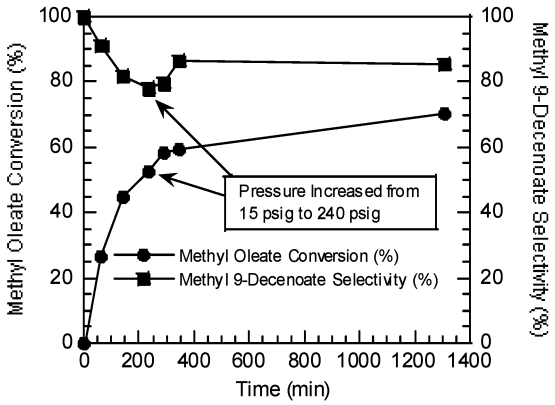


**Figure 11.** Conversion of methyl oleate (MO) in the MO ethenolysis with catalyst **1**. Conditions: 30 °C; 15 psig of ethylene initially followed by an increase to 240 psig after 237 min; 4500:1 [MO]/[**1**]; [MO] = 2.56 M.

In Figure 11, a standard [MO]/[**1**] = 4500:1 experiment was carried out at 15 psig for 4 h. The early second-order reversible model would have predicted complete decomposition of catalyst at this stage, and the literature decomposition rate of **6**[44] would have predicted <25% active catalyst. After 4 h, the pressure was raised to 240 psig to see if any shift in conversion/selectivity is observed due to the presence of active catalyst. As can be clearly seen in Figure 11, a significant increase in both is observed, demonstrating that catalyst activity is still present at this stage in the reaction.

In the hopes of developing a simple NMR test for catalyst stability, **1** and 1-decene were combined in $C_6D_6$ in an NMR tube with $Ph_3PO$ as an internal standard. The concentration of **1**, **5**, **6**, and total carbene over time was measured by $^{31}P$ NMR, as illustrated in Figure 12. Similar to the results observed by Ulman and Grubbs,[48] the initially formed alkylidene intermediate **5** rapidly converts to a majority of methylidene in under 2 h. In this study, the mixture was monitored for approximately 24 h to measure the rate of catalyst decomposition. As can be seen in Figure 12, a half-life of closer to 24 h is observed, compared to the expected 160 min based on the previous report by Grubbs (estimated based on extrapolation to room temperature). When this experiment was run with methyl oleate instead of 1-decene to limit the formed ruthenium intermediate to only alkylidenes **4**/**5**, a significantly longer lifetime (2.7 days) is observed for the alkylidene (Figure 13). This validates

(48) Ulman, M.; Grubbs, R. H. *Organometallics* **1998**, *17*, 2484.

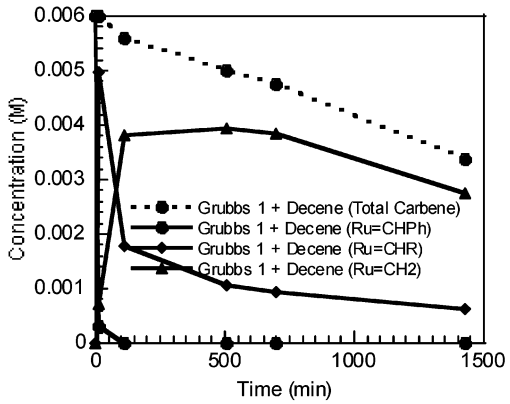


**Figure 12.** Concentration profile of ruthenium benzylidene, alkylidene, methylidene, and total carbene from catalyst **1** after treatment with 1-decene in toluene-$d_8$ with $Ph_3PO$ as an internal standard. Conditions: 30 °C; 50:1 [1-decene]/[**1**]; [1-decene] = 0.30 M.

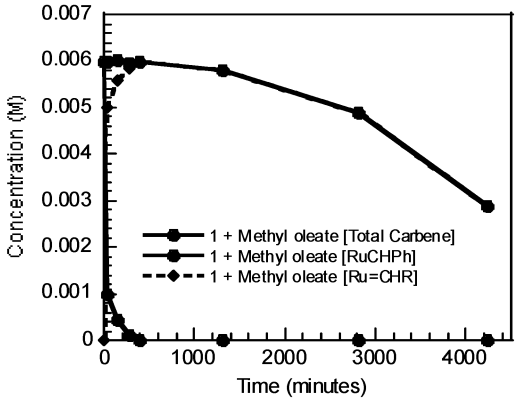


**Figure 13.** Concentration profile of ruthenium benzylidene (**1**), alkylidenes (**4**/**5**), methylidene (**6**), and total carbene from catalyst **1** after treatment with methyl oleate (MO) in toluene-$d_8$ with $Ph_3PO$ as an internal standard. Conditions: 30 °C; 50:1 [MO]/[**1**]; [MO] = 0.30 M.



the assumption present in the kinetic model that alkylidene complex decay could be ignored under these conditions. Although not directly comparable to the methyl oleate ethenolysis experiments, these NMR studies allow the facile monitoring of **1**, **4**, **5**, and **6** in the presence of olefins and the qualitative measurement of their lifetimes.

The results in Figures 12 and 13 call into question whether even the extended lifetimes reported in the literature are long enough when olefinic substrates are present. If the catalyst decay were slower than this literature value, it would imply an even more severe product inhibition effect to account for the observed rate decrease. Studies are underway to measure catalyst decomposition in situ to completely decouple the effect of product inhibition and decomposition on the observed decrease in catalyst productivity with increased conversion.

**Computational Studies**. In an attempt to better refine the kinetic model by limiting the number of necessary assumptions and guiding the direction for potential solutions, a significant effort in quantum-chemical modeling has been brought to bear on the thermodynamics of the complete catalytic cycle. Prior computational literature of the Grubbs catalyst system **1**[49−52] only covers selected parts of the present catalytic cycle. All calculations presented in this article have been done on the full $(PCy_3)_2Cl_2Ru{=}CHR$ catalyst (**1**). Methyl oleate is a long-chain molecule with a relatively small, chemically active, portion (the internal double bond). Therefore, a smaller analogue of methyl oleate (4-octene) has been utilized to compute activation barriers involving internal olefins and 1-pentene to model reactions involving the α-olefins methyl 9-decenoate and 1-decene.

In the present catalytic system, there are manifold reaction pathways, involving ethylene and terminal and internal olefins, as well as cis and trans species of internal olefins. All these basically start and end with a 14e active complex, which is in equilibrium with a pool of unreactive 16e phosphine-ligated precatalyst. Considering the two ends of the methyl oleate molecule to be chemically equivalent (assumption verified by experiment and computation;[53] see Figure 26 in the Appendix), there are 27 distinct chemical species present in the reaction mixture at any given time, not counting any catalyst decay products. These species are connected by a network of 48 elementary reactions with unique rate constants. In the following, a first-principles assessment of each of those reaction pathways is presented, starting with the simplest (degenerate ethylene metathesis). For each reaction pathway, how the particular pathway affects the overall behavior of the catalytic system will be discussed and compared with previous experimental results. The three-dimensional molecular geometries will not be depicted, except for a few prototypical ones, for space-saving reasons. The active site geometries for the 14e and 16e ruthenium species have been well characterized by Cavallo[49] at a similar level of theory and will not be described here any further.

Geometries of **6** and alkylidene complex **10** follow the pattern shown in Figure 14 and are in accord with those in the literature.[49−52]

Geometries of the 14e complexes produced by phosphine dissociation are shown in Figure 15. They are intermediate between a butterfly and a tetrahedral structure, with the Cl atoms lying approximately trans to each other. Metathesis chemistry has been found to happen exclusively by attachment of olefins to the 14e Ru complexes. No evidence for metathesis chemistry by attachment to the 16e bis-phosphine complexes has been found.[54]

(49) Cavallo, L. *J. Am. Chem. Soc.* **2002**, *124*, 8965.
(50) Adlhart, C.; Chen, P. *Angew. Chem., Int. Ed.* **2002**, *41*, 4484.
(51) Bernardi, F.; Bottoni, A.; Miscione, G. P. *Organometallics* **2003**, *22*, 940.
(52) Fomine, S.; Vargas, S. M.; Tlenkopatchev, M. *Organometallics* **2003**, *22*, 93.
(53) Several test calculations were done in which analogous reactions, differing only in the carbene substitutent ($Ru{=}(CH_2)_7CH_3$ vs $Ru{=}(CH_2)_7COOMe$), were examined. The reaction energies of both carbene species were identical to within the resolution of the method employed here (i.e., approximately 1 kJ/mol). The same is, however, not true if $PMe_3$ is employed as a ligand. For the $PMe_3$ analogue of catalyst **1**, the $Ru{=}(CH_2)_7COOMe$ species is 7 kJ/mol lower in energy than the $Ru{=}(CH_2)_7CH_3$ species, because the ester forms a chelate bond to the Ru center. This is not observed for catalyst **1**. Note that for smaller ligands such as $PMe_3$, metathesis chemistry by coordination of olefins to the 16e bisphosphine complexes was indeed found, as was also shown recently by Fomine[52] and Bernardi.[51]
(54) Note that for smaller ligands such as $PMe_3$, metathesis chemistry by coordination of olefins to the 16e bisphosphine complexes was indeed found, as was also shown recently by Fomine[52] and Bernardi.[51]

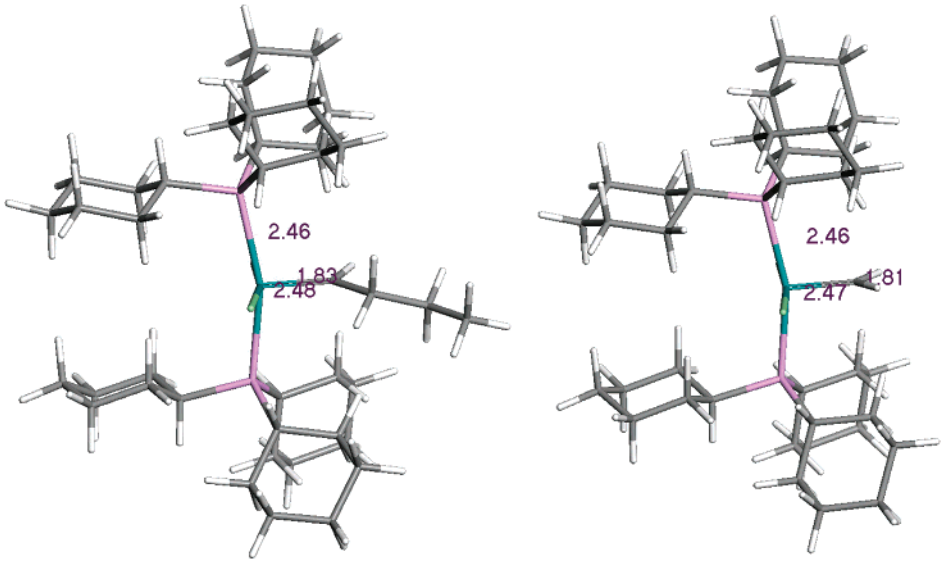


**Figure 14.** 16e Ru alkylidene complex **10** (left) and 16e Ru methylidene complex **6** (right).

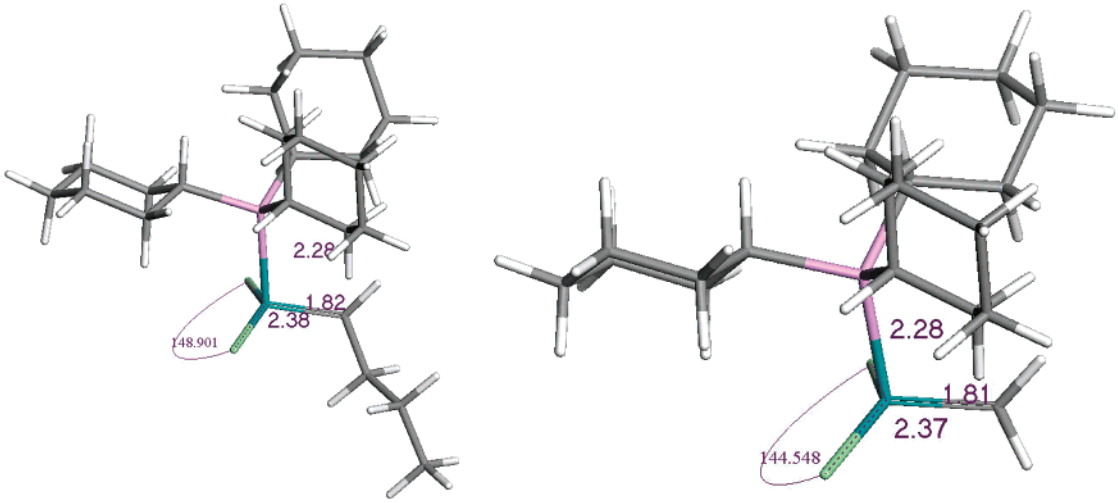


**Figure 15.** 14e Ru alkylidene complex **11** (left) and 14e Ru methylidene complex **9** (right).

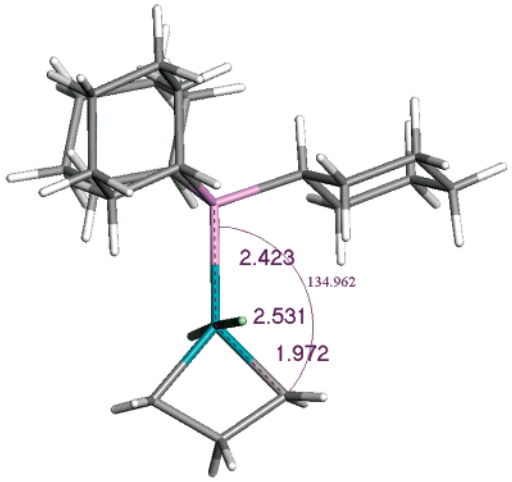


**Figure 16.** Unsubstituted metallacycle.

All metallacyclic ground and transition states follow the basic bonding pattern shown in Figure 16 for the unsubstituted metallacycle. Substitution on any of the metallacycle carbon atoms does not cause any substantial puckering of the ring (1−5° out of the plane).

**A. Reactions That Influence the Product Distribution. (a) Conversion of Internal Olefin to Alkylidene with Internal Olefin.** The productive section of the catalytic cycle consists of cleavage of internal olefin (which may be cis or trans) by **6**. Figure 17 illustrates the total energy of the system along this reaction path, which corresponds to the first equation in Scheme 9.

The salient features of productive olefin cleavage are as follows.

(1) The dominant kinetic feature is the dissociation of the phosphine ligand from the Ru alkylidene **10** and the Ru methylidene **6**.

(2) Once the 14e methylidene **9** is formed, the conversion process from internal to terminal olefin proceeds essentially downhill.

(3) Cis and trans conversion pathways are similar energetically, with the cis pathway being more exothermic, due to relaxation of steric strain.

(4) The 14e Ru alkylidene complex **11** is substantially

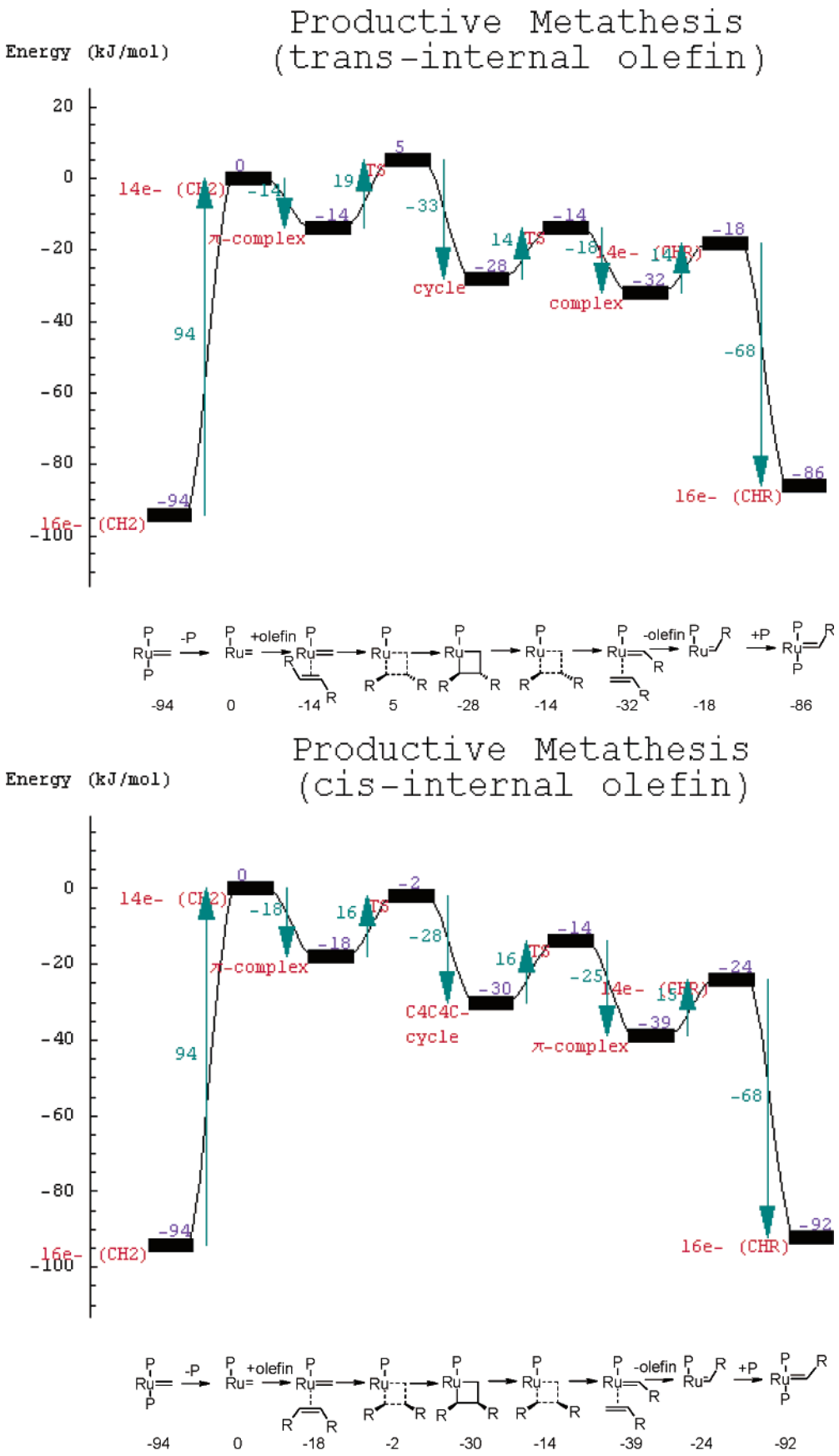


**Figure 17.** Density functional energy (kJ/mol) as a function of the reaction coordinate for the formation of alkylidene **10** from methylidene **6** with internal olefin.

lower in energy than the 14e methylidene complex **9**, favoring the alkylidene by 18 and 24 kJ/mol (trans and cis, respectively).

(5) The preference of the Ru alkylidene species **11** over the Ru methylidene complex **9** is, however, overwhelmed by the more exothermic phosphine capture energy of **9**.

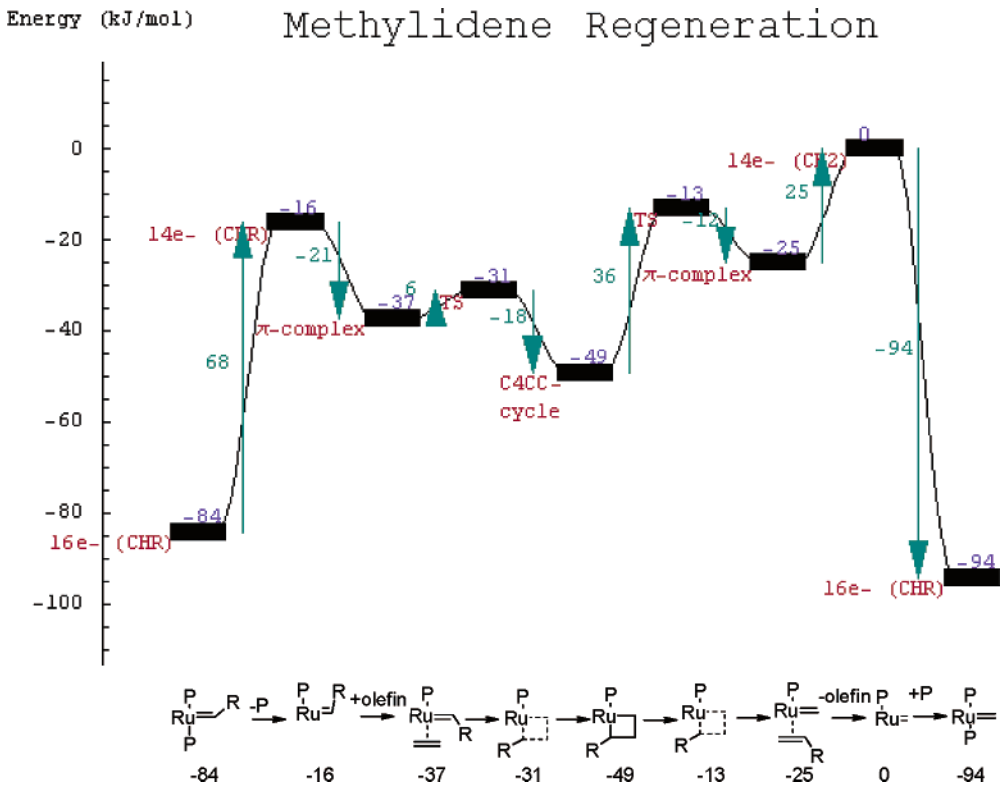


**Figure 18.** Density functional energy (kJ/mol) as a function of the reaction coordinate for the formation of alkylidene **10** from methylidene **6** with terminal olefin.

The obvious rate-determining step is the dissociation of the $PCy_3$ ligand from **6**. The dissociation of phosphine from **10** is endothermic by just 68 kJ/mol, whereas the analogous process for **6** costs 94 kJ/mol. These values are in good agreement with the values derived by Cavallo,[49] who estimated the binding energy of $PCy_3$ to the 14e Ru alkylidene to be ~60 kJ/mol. This reduction of phosphine binding energy from Ru methylidene to Ru alkylidene is partly due to electronic and steric factors: the fact that phosphine binds less strongly to the alkylidene than to the methylidene is also observed, though to a lesser extent, for $PMe_3$ (106 kJ/mol for dissociation from methylidene vs 93 kJ/mol from alkylidene). Since $PMe_3$ is too small to cause nonbonded interactions with the alkylidene group, it appears that there are some electronic effects favoring phosphine binding to methylidene over alkylidene.

The slight prevalence of the cis over the trans pathway is due to the fact that the cis internal olefin releases more strain energy on metallacycle formation than the trans internal olefin. The close resemblance of cis and trans pathways justifies the combined treatment in Kinetic Modeling Studies. The energetic preference of **6** over **10** also partially explains why the empirical model gives a higher methylidene concentration over the course of the reaction.

**(b) Regeneration of Ru Methylidene with Ethylene.** Figure 18 illustrates the regeneration of **6** from **10** with ethylene, equivalent to the second reaction in Scheme 9. The reaction equilibrium between 14e species **9** and **11** lies strongly on the side of the alkylidene **11** by 16 kJ/mol, which corresponds to approximately a 500-fold prevalence of **11** over **9** at 303 K. The same pattern is observed in Figure 17.

Regeneration of **6** from **10** involves complexation of ethylene to the 14e alkylidene **11**. This process is exothermic by 21 kJ/mol. Cavallo found 23 kJ/mol exothermicity for the same process.[49]

Examination of Figure 18 shows the following.

(1) As observed in Figure 17, the phosphine dissociation appears to be the high-barrier process.

(2) The stability of the monosubstituted metallacycle is substantially higher (−49 kJ/mol below the Ru methylidene **6** + terminal olefin) than the stability of the disubstituted metallacycles in Figure 17.

(3) Considering the overall shape of the reaction profile, it appears that the overall activation barrier for the reaction $(PCy_3)_2RuCHR$ + ethylene ⇌ $(PCy_3)_2RuCH_2$ + terminal olefin is lower (approximately 84 kJ/mol) than the activation barrier for the reaction $(PCy_3)_2RuCH_2$ + MO ⇌ $(PCy_3)_2RuCHR$ + terminal olefin (approximately 94 kJ/mol), as shown in Figure 17.

(4) The reaction of ethylene with Ru alkylidene **10** is dominated by the dissociation of phosphine.

**(c) Cis/Trans Isomerization of Internal Olefins with Alkylidene.** Another one of the observed reactions in the methyl oleate/ethylene reaction mixture is cis/trans isomerization of internal olefins and concomitant scrambling of $(CH_2)_7COOMe$ and $(CH_2)_7CH_3$ chain ends. Reaction of alkylidene with internal olefins can result in cis/trans isomerization of the internal olefin if the olefin adds to form a trisubstituted 2,3,4-(*cis*/*trans*)-metallacyclobutane. Thermodynamically, cis/trans isomerization lies toward the side of the trans internal olefin by 7 kJ/mol at the present level of theory[55] (Figure 19). The *cis*/*trans*-metallacyclobutane formed in this reaction lies well above the dissociation limit (17 kJ/mol), which is much higher compared to the values for

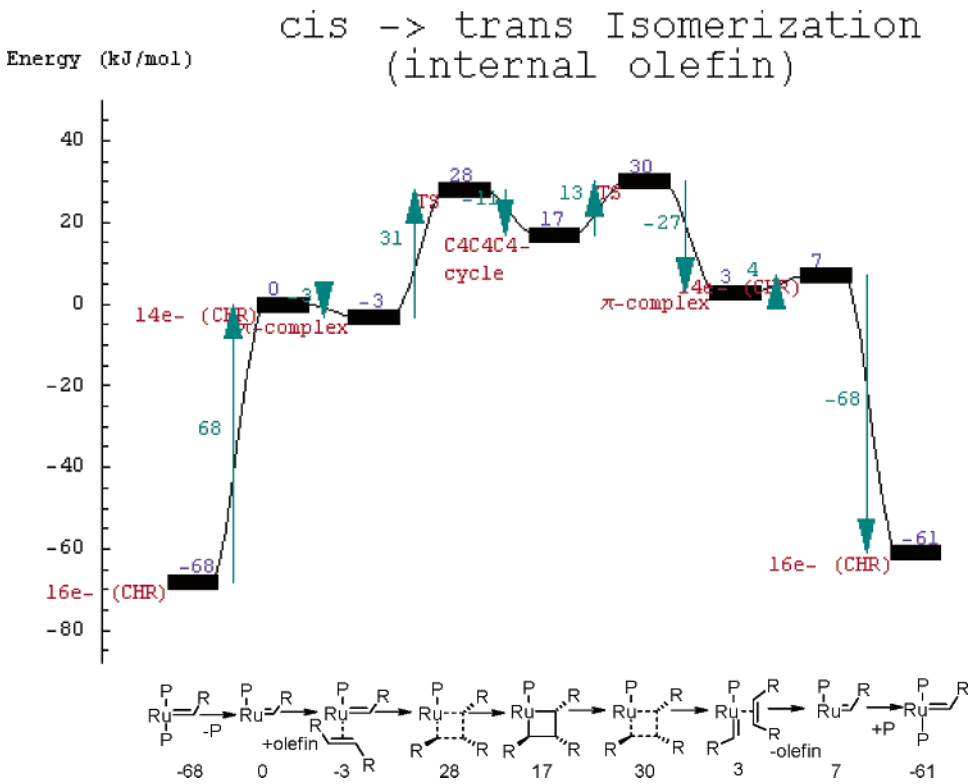


**Figure 19.** Density functional energy (kJ/mol) as a function of the reaction coordinate for the cis/trans isomerization of terminal olefin with alkylidene **10**.

the less substituted metallacycles encountered in Figures 17 and 18. This is in line with the experimental observation that cis/trans isomerization and internal olefin scrambling is much slower than the productive reactions, such as productive metathesis or catalyst regeneration.

**(d) Scrambling of Internal Olefins without Cis/Trans Isomerization.** Scrambling metathesis of internal olefins may occur when trans olefins add to produce 2,3,4-(trans/trans)-substituted metallacycles or cis olefins add to produce 2,3,4-(cis/cis)-substituted metallacycles.

In the present case of methyl oleate metathesis, the degenerate metathesis mechanisms shown in Figure 20 have the potential to produce 9-octadecene and dimethyl 9-octadecene-1,18-dioate from methyl oleate. Both degenerate reaction pathways include metallacyclobutane structures that are above the dissociation limit (7 kJ/mol for trans/trans and 25 kJ/mol for cis/cis).

Comparing the stabilities of the three pathways that include trisubstituted metallacyclobutanes (Figures 19 and 20), one notes that in all three of them the metallacyclobutane structures lie above the dissociation limit—thus, the reactions involving these metallacycles are the slowest of all those investigated here. Furthermore, one notes that the trans/trans metallacycle is by far the most stable one (7 kJ/mol above dissociation limit, Figure 20, top), followed by the cis/trans metallacycle (17 kJ/mol above limit, Figure 19) and the cis/cis metallacycle, which is the most unstable (25 kJ/mol above dissociation limit, Figure 20, bottom). These data support the assumption used in the kinetic modeling that homometathesis kinetics can be ignored for all practical intent with catalyst **1** under these conditions.

**B. Reactions That Do Not Influence the Product Distribution.** Reactions that do not influence the observed product distribution are not detectable by the presence or absence of particular reaction products. However, they may distract active ruthenium centers from productive reactions and thus influence the course and kinetics of the reaction.

**(a) Degenerate Reaction of Ethylene with Methylidene.** Figure 21 shows the behavior of the total energy during the process of degenerate ethylene metathesis, which is a side reaction that does not change the product distribution. The obvious rate-determining step is the dissociation of the $PCy_3$ ligand from **6**. The activation energy for this process (94 kJ/mol) is slightly higher than the experimental value measured for $PCy_3$ loss from **1** (83 kJ/mol).

The subsequent capture of ethylene by the 14e methylidene **9** (−32 kJ/mol) is much less exothermic than capture of phosphine. Surprisingly, the metallacyclobutane is formed from the ethylene $\pi$-complex with an almost negligible barrier of only 5 kJ/mol. Its formation, relative to the $\pi$-complex, is somewhat exothermic at −26 kJ/mol. With the small energetic barrier between

(55) An additional G2MP2 calculation with the Gaussian98 program puts the cis/trans conversion energy at −5.0 kJ/mol, in close agreement with the 7 kJ/mol density-functional value. Frisch, M. J.; Trucks, G. W.; Schlegel, H. B.; Scuseria, G. E.; Robb, M. A.; Cheeseman, J. R.; Zakrzewski, V. G.; Montgomery, J. A., Jr.; Stratmann, R. E.; Burant, J. C.; Dapprich, S.; Millam, J. M.; Daniels, A. D.; Kudin, K. N.; Strain, M. C.; Farkas, O.; Tomasi, J.; Barone, V.; Cossi, M.; Cammi, R.; Mennucci, B.; Pomelli, C.; Adamo, C.; Clifford, S.; Ochterski, J.; Petersson, G. A.; Ayala, P. Y.; Cui, Q.; Morokuma, K.; Malick, D. K.; Rabuck, A. D.; Raghavachari, K.; Foresman, J. B.; Cioslowski, J.; Ortiz, J. V.; Stefanov, B. B.; Liu, G.; Liashenko, A.; Piskorz, P.; Komaromi, I.; Gomperts, R.; Martin, R. L.; Fox, D. J.; Keith, T.; Al-Laham, M. A.; Peng, C. Y.; Nanayakkara, A.; Gonzalez, C.; Challacombe, M.; Gill, P. M. W.; Johnson, B. G.; Chen, W.; Wong, M. W.; Andres, J. L.; Head-Gordon, M.; Replogle, E. S.; Pople, J. A. *Gaussian 98*, revision A.6; Gaussian, Inc.: Pittsburgh, PA, 1998.

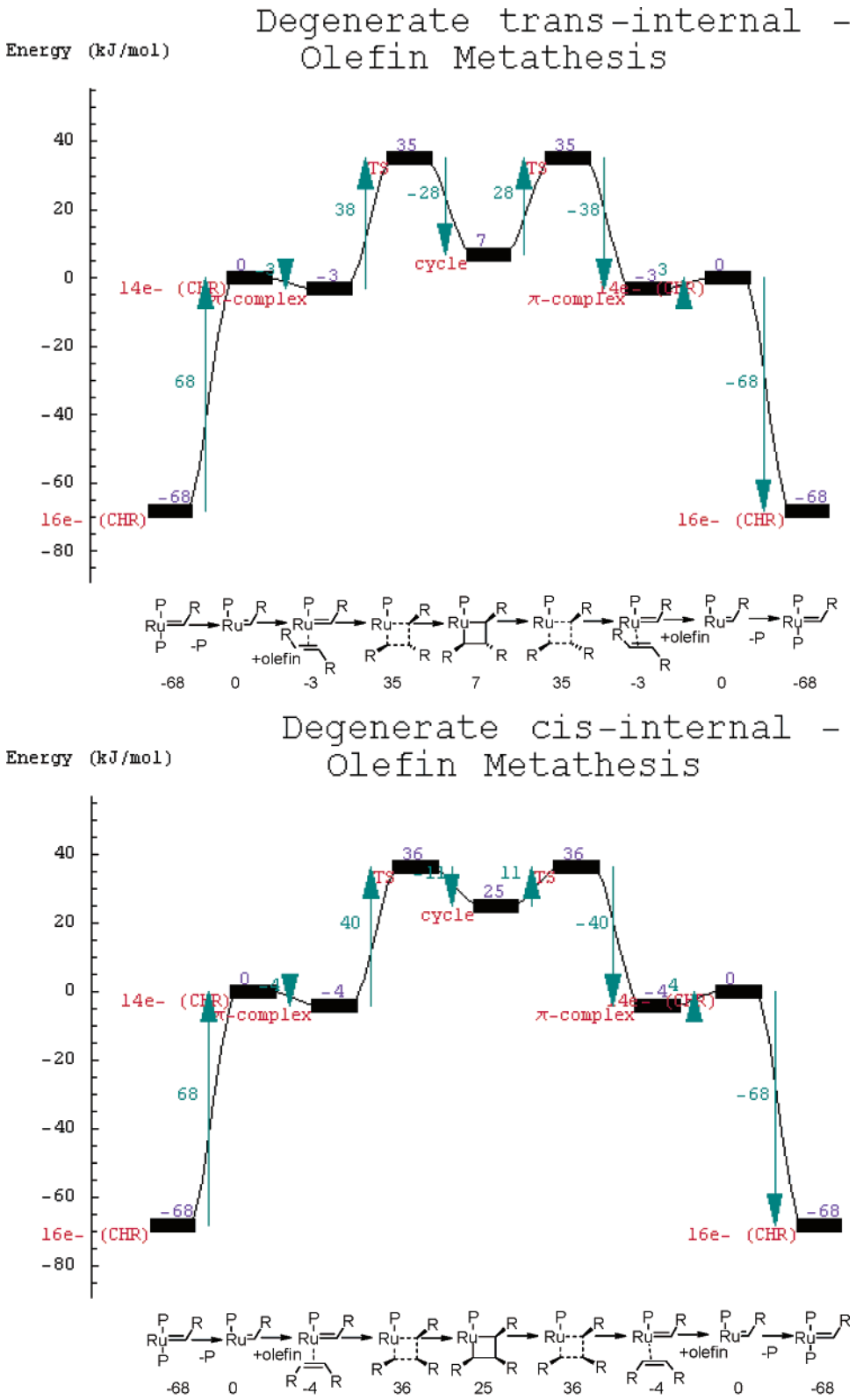


**Figure 20.** Degenerate metathesis of internal olefin with alkylidene.

$\pi$-complex and metallacycle, the degenerate ethylene metathesis reaction can be regarded as a competition between phosphine- and ethylene-capture equilibria of the 14e methylidene **9**, as has been previously described.[17]

As the unsubstituted metallacycle in Figure 21 is substantially higher in energy than the phosphine-substituted 16e complex **6** but substantially lower than the 14e compound **9** (even if the entropic contribution to the equilibrium—approximately 40 kJ/mol at room temperature—is taken into account), it therefore appears that the unsubstituted metallacycle withdraws ruthenium from the active 14e state.

**(b) Degenerate Reaction of Terminal Olefin with Methylidene.** Figure 22 illustrates the degenerate metathesis reaction of 14e methylidene **9** with terminal olefin. Despite an overall similarity, one should note that the depth of the energy well of the metallacyclo-

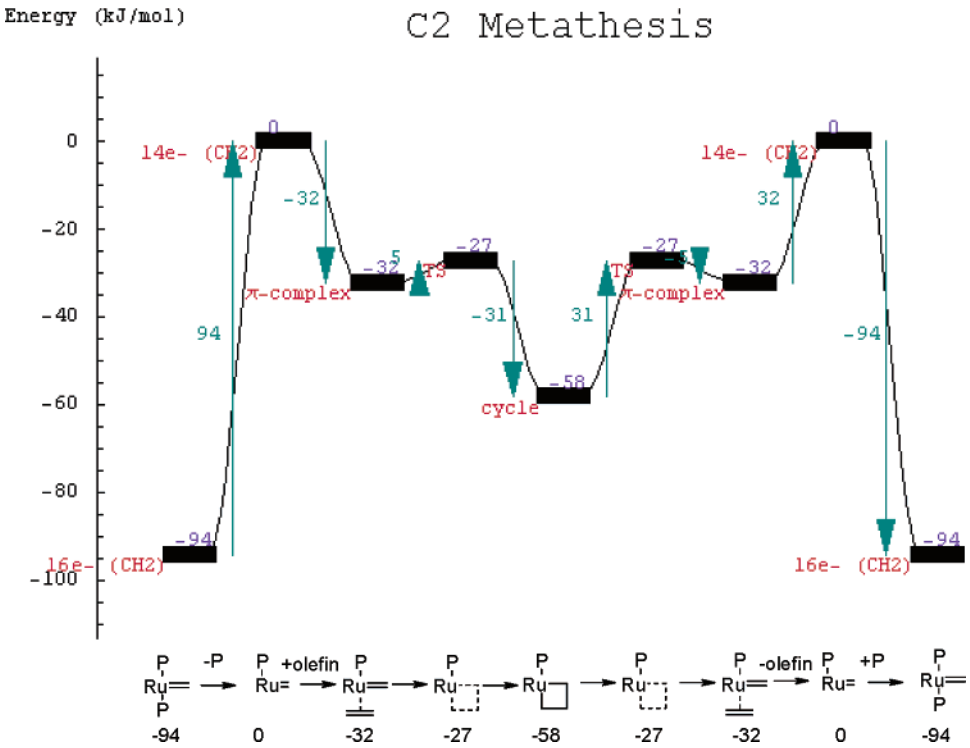


**Figure 21.** Density functional energy (kJ/mol) as a function of the reaction coordinate for the degenerate turnover of ethylene by methylidene. Numbers above bars indicate relative energies. Numbers adjacent to arrows indicate barriers.

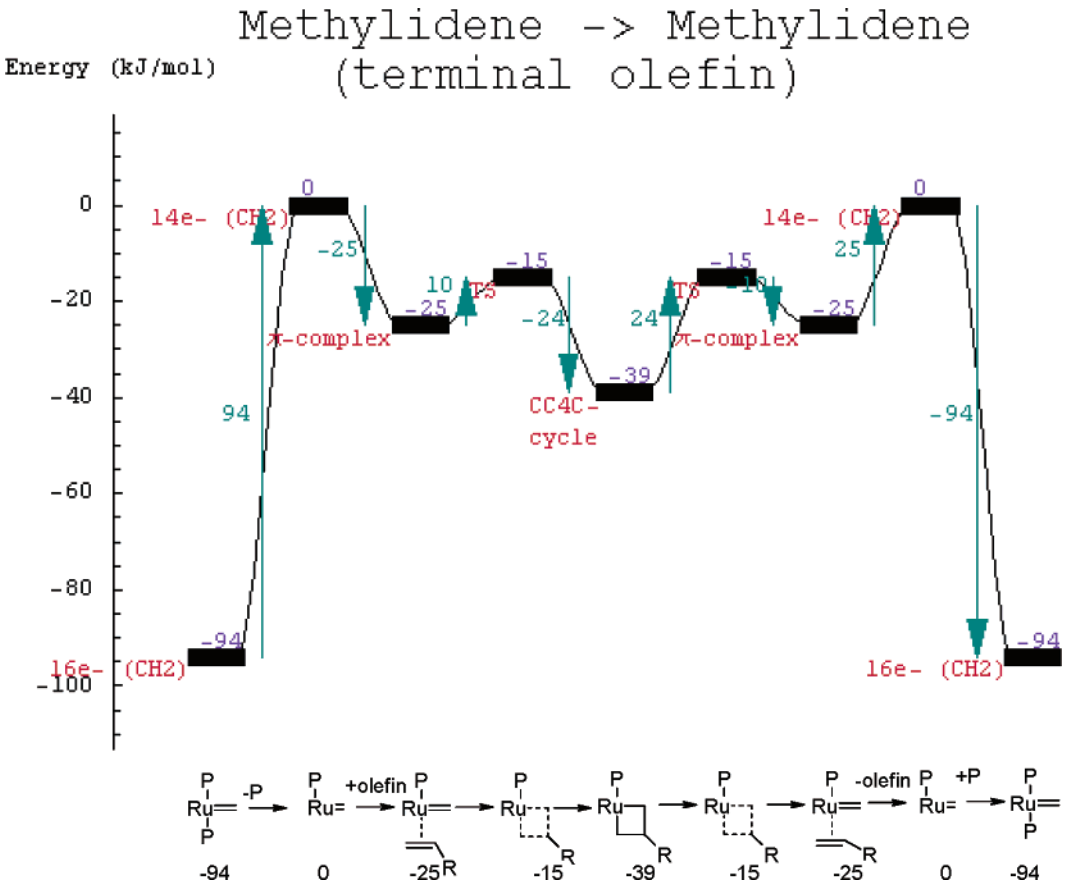


**Figure 22.** Density functional energy (kJ/mol) as a function of the reaction coordinate for the degenerate turnover of terminal olefin by methylidene.

butane has become more shallow than in Figure 21. Olefin $\pi$-complex and 3-substituted metallacyclobutane are weaker compared to their ethylene-based analogues. It appears that, at similar molar concentrations, the unsubstituted metallacycle will be strongly prevalent over the 3-substituted metallacycle. Those conclusions notwithstanding, the 3-substituted metallacycle lies 39 kJ/mol below the dissociation limit, which is of the same

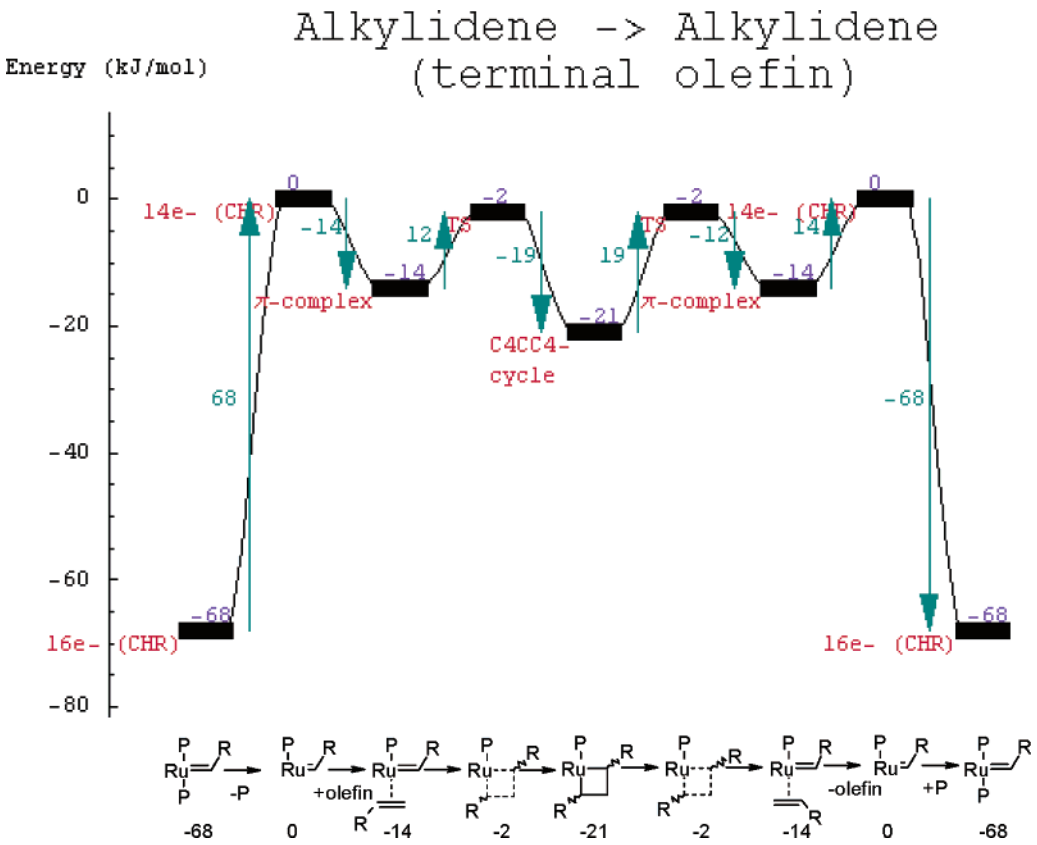


**Figure 23.** Density functional energy (kJ/mol) as a function of the reaction coordinate for the degenerate reaction of alkylidene with terminal olefin.

order of magnitude as the entropic force that counteracts bonding at room temperature (~40 kJ/mol). Bearing in mind that DFT calculations of the type performed here are usually accurate to about 10−15 kJ/mol, it may be that, in reality, the 3-substituted metallacycle forms the trap that forces the semiempirical model to include a retardation factor of [L] + $\sum$[RCH=$CH_2$]. Thus, although the present calculations do not directly predict the 3-substituted metallacycle to withdraw significant amounts of ruthenium from the productive reactions, the inaccuracy of the theory employed here would allow for this to be the case in reality.

Interestingly, the 2-alkylmetallacyclobutane formed in Figure 18 is more stable than the 3-alkylmetallacyclobutane formed in Figure 22, which agrees with Ulman's and Grubbs' conclusion[48] that the kinetically preferred metallacycle is the one with the alkyl adjacent to the metal. It appears that this is a purely electronic effect, because this trend also holds up if $PMe_3$ is substituted for $PCy_3$ (for $PMe_3$, the 3-alkyl complex lies 23 kJ/mol below terminal olefin dissociation limit, whereas the 2-alkyl complex lies 34 kJ/mol below the limit).

**(c) Degenerate Metathesis of Alkylidene with Terminal Olefin.** Alkylidene **10** formed by the productive reaction of methylidene **6** with internal olefins can react with ethylene (Figure 18) to regenerate **6** or undergo side reactions that scramble terminal and internal olefins. The latter, nondegenerate reactions of the 14e alkylidene **11** with terminal olefin are shown in Figure 20 and have been shown to be thermodynamically disfavored.

The degenerate metathesis of terminal olefin with **10** involves formation of a 2,4-substituted metallacycle, as shown in Figure 23. As both trans and cis orientations of the alkyl substituents have essentially identical total energies, Figure 23 serves to illustrate both trans and cis pathways. By virtue of being a degenerate reaction and having a relatively shallow reaction profile, this path does not seem to have the potential to greatly influence the course of the catalytic cycle.

**C. General Observations from Molecular Modeling. (a) Relative Reactivities of Olefins.** The data presented here afford us a unique opportunity to compare the relative substitution effects on the reactivity of the olefins. It is an experimentally observed fact that "*Bulkier olefins were found to react slower, and trans internal olefins were found to be slower than cis. The kinetic product of all reactions was found to be the alkylidene rather than the methylidene*".[48] According to these calculations higher substituted olefins bind less strongly to the 14e methylidene catalyst to form the metallacycle, and trans internal olefins bind less strongly to the catalyst than cis internal ones. Cis internal olefins appear to react more quickly with methylidene, since the double bond in them is exposed, rather than hidden, which allows for more facile approach to the active site. Furthermore, the steric strain on cis internal olefins appears to allow the metallacyclobutane to open more easily and it skews the equilibrium between 14e methylidene **9** and alkylidene **11** more toward the alkylidene (−24 kJ/mol for cis internal olefin as opposed to −18 kJ/mol for trans internal olefin). These results clearly support the observed kinetics for *cis*- vs *trans*-methyl oleate ethenolyis rates in Figure 24 in the Appendix. In addition, one would expect more severe product inhibition in the ethenolysis of *trans*-methyl oleate compared to *cis*-methyl oleate, due to the even larger

preference for terminal olefin versus trans olefin binding (terminal olefin preferred by 11 kJ/mol) to the 14e methylidene **9** compared to cis olefin binding (terminal olefin preferred by only 7 kJ/mol).

**(b) Relative Stabilities of Metallacycles.** A higher degree of substitution on the metallacyclobutane tends to destabilize the metallacycle relative to the unbound reactants: a 2,3-substituted metallacycle lies typically −30 kJ/mol below the methylidene/olefin dissociation limit (Figure 17), whereas the 2- or 3-monosubstituted metallacycles lie 39 and 49 kJ/mol below their methylidene/olefin dissociation limits (Figures 18 and 22). The unsubstituted metallacycle lies 58 kJ/mol below the limit (Figure 21).

**(c) Relative Stabilities of Ru Carbenes.** A common feature of all 14e methylidene/alkylidene equilibria is that they are skewed toward the side of the alkylidene. A comparative calculation using $PMe_3$ produces essentially the same trend. Since $PMe_3$ imposes very little steric hindrance upon the catalyst, the observed preference of alkylidene over methylidene appears to be a largely electronic effect. Only with the formation of terminal olefin products does a modest shift toward more methylidene occur. For the 16e complexes, the preferred binding of phosphine to the methylidene over the alkylidene intermediate results in a higher degree of **6** over **10** in the reaction mixture, which increases further with terminal olefin formation (consistent with the kinetic modeling results).

**(d) Catalyst Inhibition by Terminal Olefin.** The terminal olefin retardation in eq 2 points to a reversible pathway involving terminal olefin that withdraws ruthenium away from the active cycle. Terminal olefin is involved in several pathways in the catalytic cycle (see Figures 17, 18, 22, and 23). Only two of these pathways are explicitly considered in the semiempirical kinetic model (Figures 17 and 18). To account for the additional complexity introduced by the reactions in Figures 22 and 23, the semiempirical model features a divisor of $[L] + [RCH{=}CH_2]$, where $[RCH{=}CH_2]$ is the concentration of terminal olefin species, which reduces the amount of available ruthenium. Thus, the semiempirical model takes into account the formation of $\pi$-complexes and metallacycles that remain otherwise unaccounted for (see also Degenerate Metathesis of Terminal Olefin with Methylidene).

**Relationship between the Kinetic and Molecular Modeling Solutions.** Each of these approaches brings its own set of limitations to a complex scheme such as methyl oleate ethenolysis. Kinetic modeling of this mechanism requires the prudent choice of reasonable assumptions to limit the number of equations and thus fitting parameters to be solved for. Without these assumptions, the large number of fitting parameters increases the number of potential solutions and thus raises uncertainty, although the use of assumptions leads to another set of uncertainties. Molecular modeling can address all of the critical equations in the kinetic scheme without the need for simplifying assumptions, but as a result of the large number of variables in the system, small errors in the energy calculations can significantly affect the outcome. Taken together, the kinetic and molecular modeling approaches allow for the development of a strong understanding of complex kinetic cycle and the critical factors which influence the productive catalytic pathway.

**Table 5. Comparison of the Kinetic Parameter Estimation Using the Kinetic Model Only and Using the Kinetic Model with $K_1$ and $K_2$ Constants Derived from Molecular Modeling**

| | kinetic modeling | molecular modeling |
|---|---|---|
| $k_1$ ($min^{-1}$) | 0.0471 | 0.0307 |
| $k_{-1}$ ($min^{-1}$) | 0.0880 | 0.0682 |
| $k_2$ ($min^{-1}$) | 0.8821 | 0.9261 |
| $k_{-2}$ ($min^{-1}$) | 0.0286 | 0.0175 |
| $K_1$ | 0.53552 | 0.45 |
| $K_2$ | 30.81 | 53.00 |
| terminal olefin retardation ($k'$) | $1.69 \times 10^{-3}$ | $1.09 \times 10^{-3}$ |

To further evaluate the results from molecular modeling, the calculated $K_1$ and $K_2$ constants derived from molecular modeling ($K_1 = 0.45$ and $K_2 = 53$) have been inserted into the semiempirical kinetic model as constants, to see how they influence the overall fit to the experimental data. Table 5 lists the resulting kinetic constants from the use of $K_1$ and $K_2$ from the modeling studies compared to the kinetic modeling-only parameter estimations. The similarity of the results with the kinetic-modeling-only data and the fit with the experimental data builds support for this overall direction that has been outlined for the catalytic cycle and demonstrates the strength of these approaches for dealing with such complex systems.

## Conclusions

In an attempt to elucidate the key features of the ethenolysis of methyl oleate catalyzed by catalyst **1**, a concerted program involving experimental screening of process variable impact and kinetic analysis, kinetic modeling, and molecular modeling has been undertaken. To summarize the initial studies on the ethenolysis of methyl oleate with **1**, extremely high initial rates have been observed, even at loadings of <0.001 mol %, and high selectivities to the terminal olefin products can be achieved under mild temperatures and pressures. More importantly, productive catalyst turnovers of >15 000 have been demonstrated with **1**, far surpassing previous reports for the ethenolysis of methyl oleate. However, the rate slows significantly as conversion to terminal olefins becomes substantial. This adverse impact of terminal olefins on the catalytic cycle and catalyst productivity is complex and is the result of several parallel pathways.

As illustrated through both kinetic and molecular modeling, the terminal olefins can impact the rate of productive turnovers as a result of (1) formation of degenerate pathways for both the methylidene and alkylidene intermediates, (2) shifting of the methylidene/alkylidene equilibrium toward methylidene, thus raising the rate of catalyst decomposition at the same time that product inhibition is dominant, and (3) increased competition with internal olefin for $\pi$-complexation (and/or metallacycle formation) with the 14e ruthenium complexes **7**−**9**. This third pathway can be quantified using molecular modeling, where for the 14e ruthenium methylidene **9**, the ordering for the exotherm from $\pi$-complexation of olefin is ethylene (−32 kJ/mol) > terminal olefin (−25 kJ/mol) > internal olefin (trans,

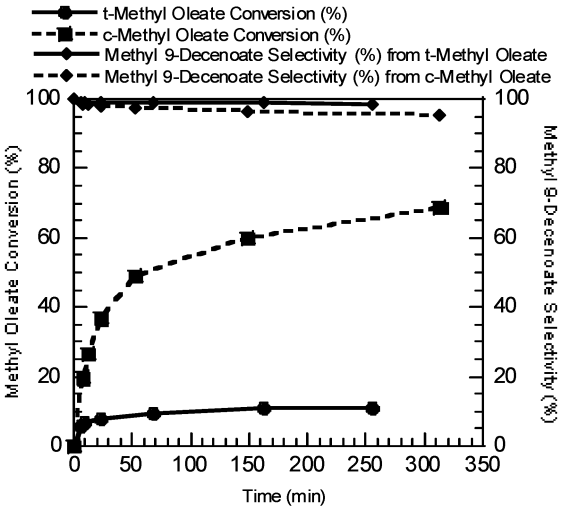


**Figure 24.** Comparison of methyl oleate conversion in MO ethenolysis with catalyst **1** using *cis*-MO and *trans*-MO. Conditions: 30 °C; 60 psig of ethylene; 4500:1 [MO]/[**1**]; [MO] = 1.483 M (in tetradecane).

−14 kJ/mol; cis, −18 kJ/mol). Obviously, ethylene binding is the most preferred, but in order for productive metathesis to occur between internal olefin and **6**, internal olefin needs to successfully compete with the other olefins in the reaction for binding and therefore terminal olefins (2 mol produced from each internal olefin) dramatically retard this step. A similar analysis of the relative metallacycle energetics would lead to the same trend. The above pathways, coupled with the known instability of the methylidene intermediate, lead to the decrease in observed rate with increased time/conversion. Other potential roles of terminal olefin in the reduction of catalyst activity are currently under investigation.

Although this impact of terminal olefins on catalyst productivity is detrimental, the conclusion that one reaches is that the initially predicted rates of catalyst deactivation were far too rapid and that catalyst **1** is active at least on the order of hours for this chemistry. The development of processes for either selective product removal to drive the reaction and limit product inhibition or for catalyst removal/recycling at lower conversions, thus maximizing the catalyst initial productivity, are currently underway, on the basis of the conclusions from this study. We are optimistic that the ethenolysis of methyl oleate could soon achieve economical turnovers and open up a wealth of new chemistries and product opportunities from renewable seed oils.

**Acknowledgment.** We thank Pat Nugent and Zenon Lysenko for their support of this project and their contributions to the research in the report and Wayde Konze, Francis Timmers, Eric Lucas, Don Morrison, Michael Tulchinsky, Brian Roesch, Rik Tuinstra, Cynthia Rand, and Tom Newman for helpful discussions.

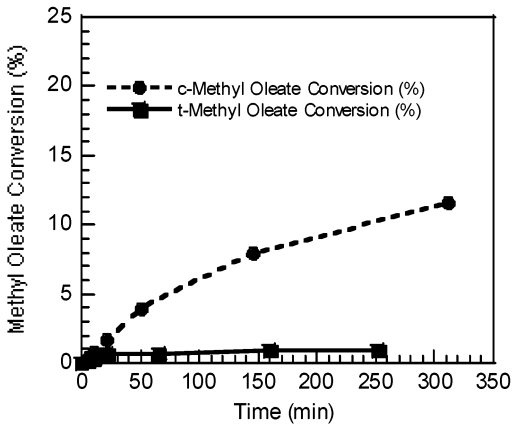


**Figure 25.** Comparison of methyl oleate conversion in MO homometathesis with catalyst **1** using *cis*-MO and *trans*-MO. Conditions: 30 °C; 4500:1 [MO]/[**1**]; [MO] = 1.483 M (in tetradecane).

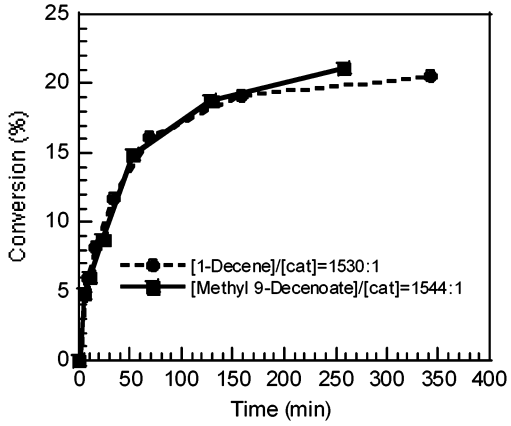


**Figure 26.** Conversion of either 1-decene or methyl 9-decenoate self-metathesis using catalyst **1**. Conditions: 30 °C; 50 psig of nitrogen; 1530:1 [1-decene]/[**1**] and 1544:1 [methyl 9-decenoate]/[**1**]; [1-decene] = 4.30 M and [methyl 9-decenoate] = 3.35 M, where both were run essentially neat with a small amount of added internal standard.

We gratefully acknowledge financial support for this research effort from the Department of Energy and The Dow Chemical Company Industrial Biotechnology Business through a joint DOE contract (DE-FC07-01ID14213).

## Appendix

Figures 24 and 25 give comparisons of methyl oleate conversion in MO ethenolysis and homometathesis, while Figure 26 shows the conversion of either 1-decene or methyl 9-decenoate.

**Supporting Information Available:** Tables of laboratory kinetic data and kinetic model fitting results, ethylene solubility studies, and coordinates from molecular modeling. This material is available free of charge via the Internet at http://pubs.acs.org.

OM0341799